Stability *vs.* Activity in Electrocatalytic Hydrogen Production and Magnetic Studies of Mononuclear Labile Cu(II) and Ni(II) Complexes

Maria A. Bhatti,[a] Luca M. Carrella, [a] Carsten Streb,[a] Eva Rentschler [a*] and Sriram Sundaresan [a,b*]

[a]Department Chemie, Johannes-Gutenberg-Universität Mainz, Duesbergweg 10–14, 55128 Mainz, Germany.

[b]Institute of Physics, Czech Academy of Sciences, Cukrovarnická 10, 162 00 Prague, Czech Republic.

Email: rentschl@uni-mainz.de and sundaresan@fzu.cz

Electronic Supplementary Information

Table of Contents

S1. NMR spectra

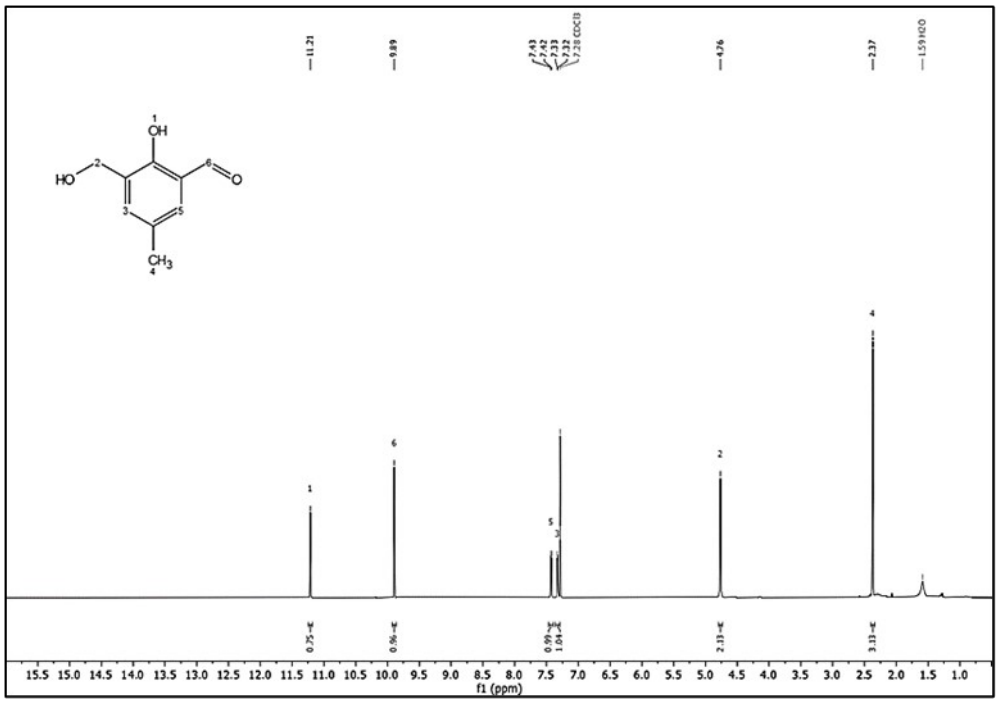

Figure S 1[1]H-NMR spectrum of of 2-hydroxy-3-(hydroxymethyl)-5-methylbenzaldehyde in $CDCl_3$.

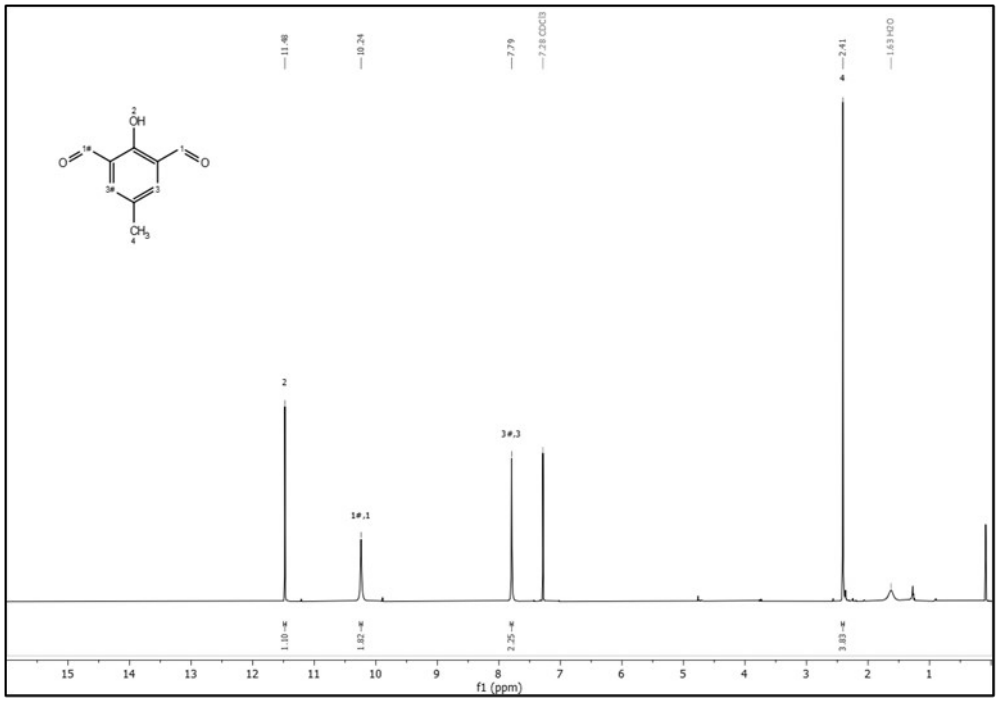

Figure S 2 [1]H-NMR spectrum of of 2-hydroxy-5-methylisophthalaldehyde in $CDCl_3$.

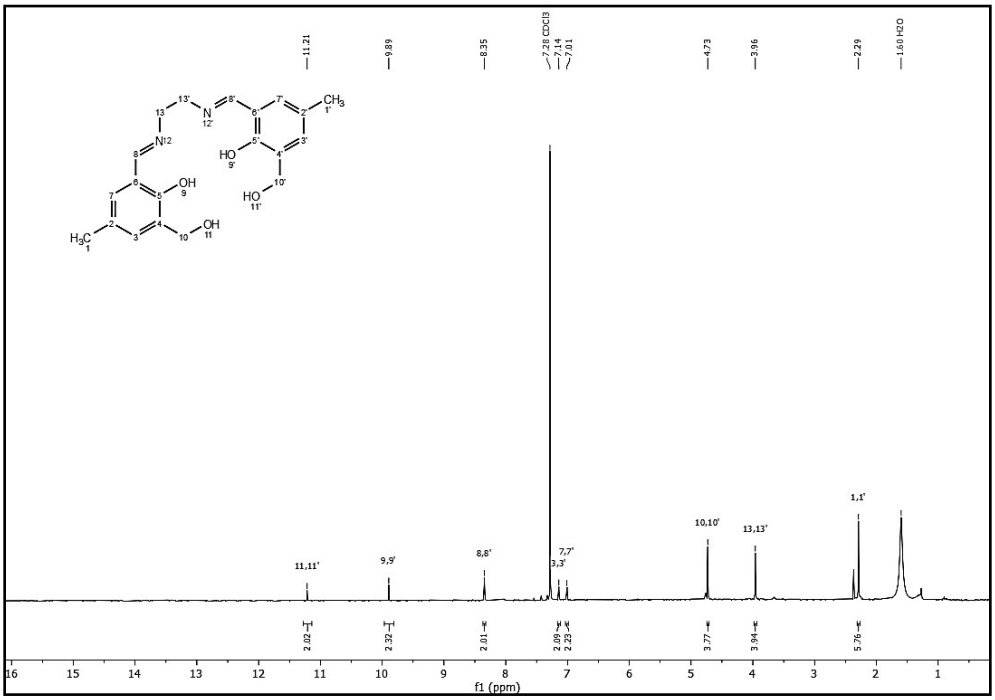

Figure S 3 ^{1}H-NMR spectrum of schiff-base ligand 6,6'-((1E,1'E)-(ethane-1,2-diylbis(azaneylylidene))bis(methaneylylidene))bis(2-(hydroxymethyl)-4-methylphenol) (**H_4L**) in $CDCl_3$.

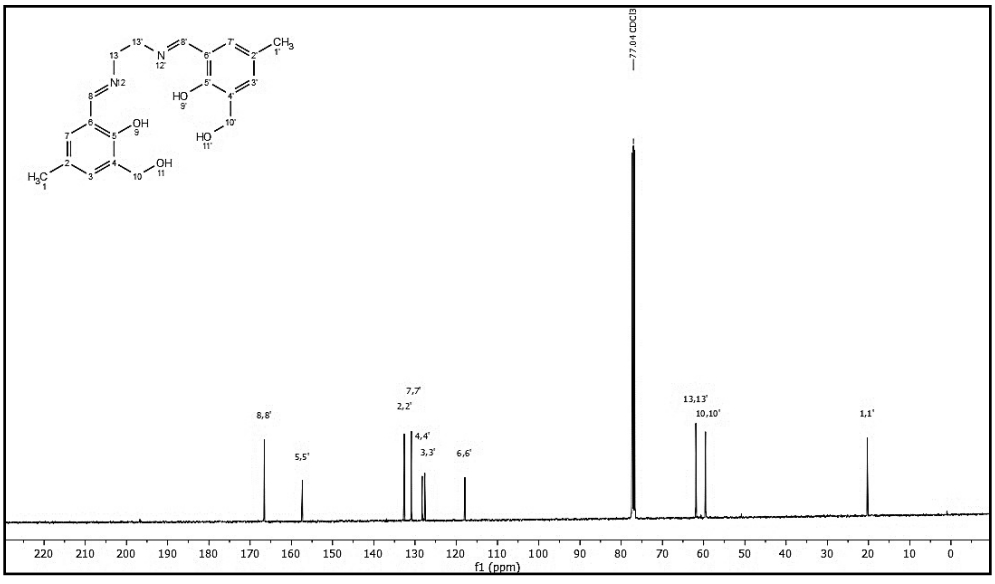

Figure S 4 ^{13}C NMR spectrum of schiff-base ligand 6,6'-((1E,1'E)-(ethane-1,2-diylbis(azaneylylidene))bis(methaneylylidene))bis(2-(hydroxymethyl)-4-methylphenol) (**H_4L**) in $CDCl_3$.

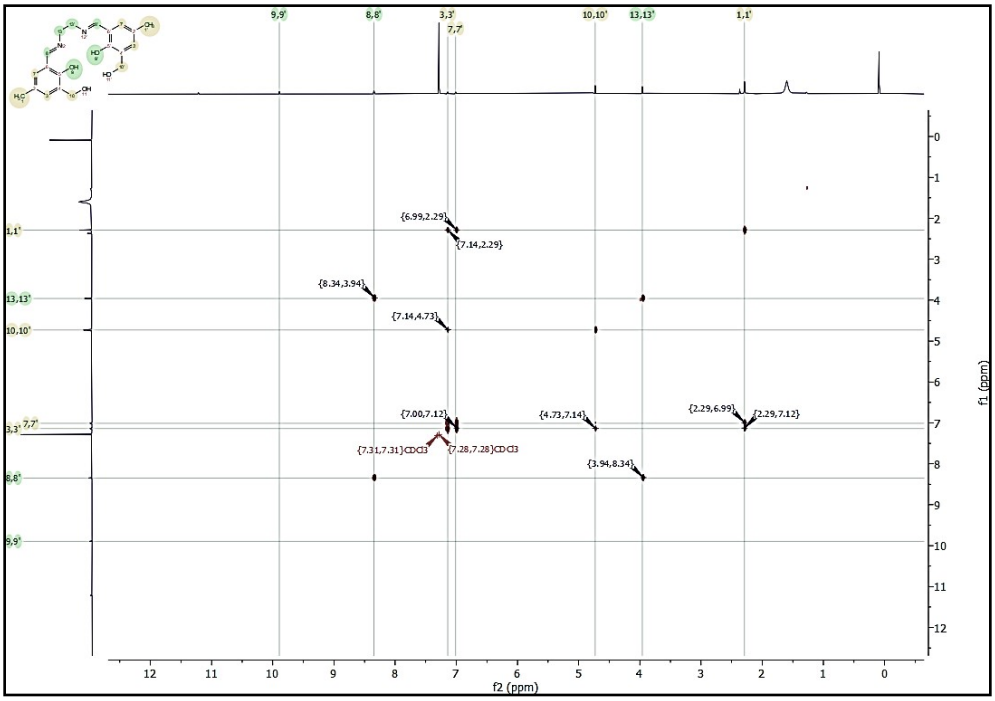

Figure S 5 ^{1}H-^{1}H COSY NMR spectrum of schiff-base ligand 6,6'-((1E,1'E)-(ethane-1,2-diylbis(azaneylylidene))bis (methaneylylidene))bis(2-(hydroxymethyl)-4-methylphenol) (**H_4L**) in $CDCl_3$.

S2. IR spectra

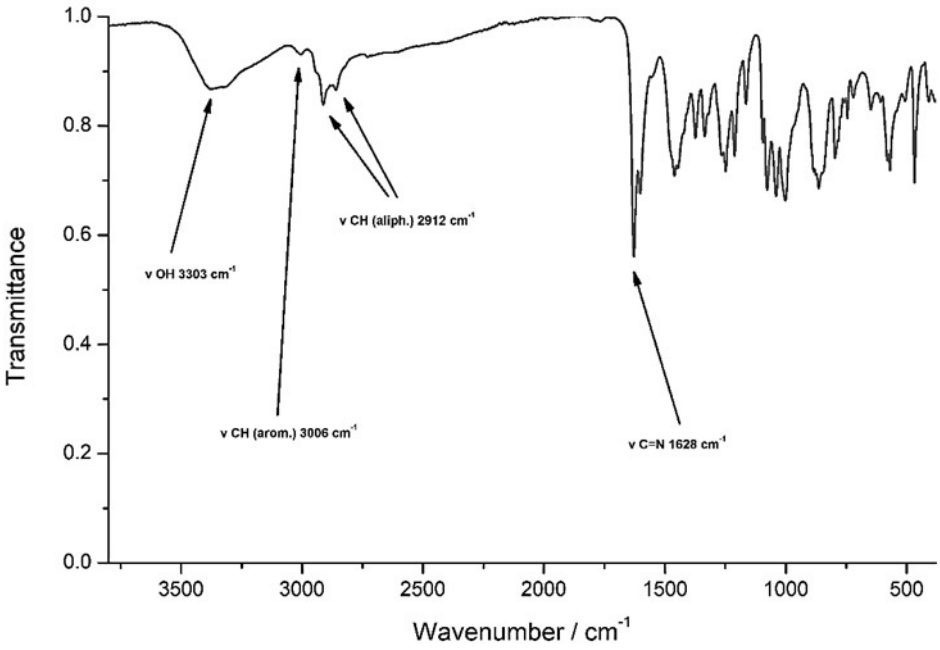

Figure S 6 IR spectrum of schiff-base ligand 6,6'-((1E,1'E)-(ethane-1,2-diylbis(azaneylylidene))bis(methaneylylidene)) bis(2-(hydroxymethyl)-4-methylphenol) (**H_4L**) with associated IR bands.

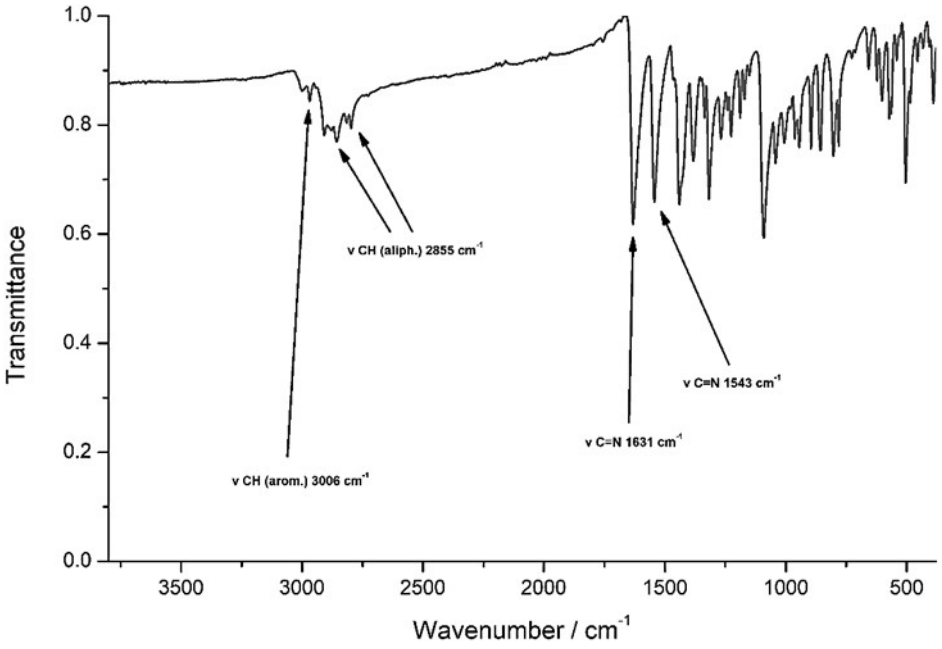

Figure S 7 IR spectrum of copper complex $[Cu^{II}L^{Me}] \cdot 1.5\ H_2O$ (**C1**) with associated IR bands.

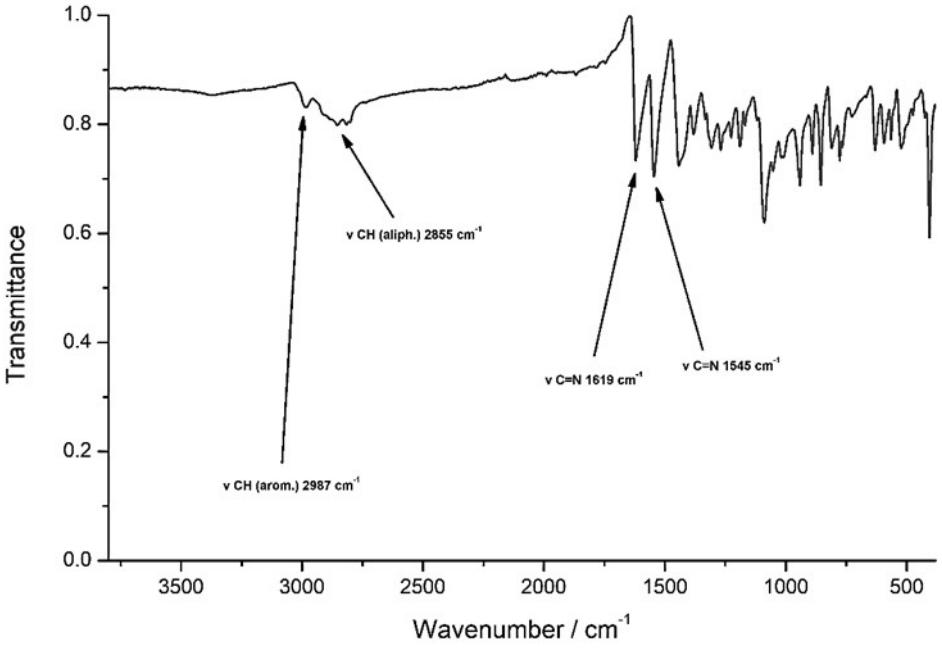

Figure S 8 IR spectrum of copper complex $[Ni^{II}L^{Me}] \cdot 3\ H_2O$ (**C2**) with associated IR bands.

S3. Crystallographic data

Table S 1 X-ray crystallographic data for complex $[Cu^{II}L^{Me}] \cdot 1.5\ H_2O$ (**C1**) and $[Ni^{II}L^{Me}] \cdot 3\ H_2O$ (**C2**).

Compound	**C1**	**C2**
Empirical formula	$C_{22}H_{26}CuN_2O_4$	$C_{22}H_{26}NiN_2O_4$
Formula weight / $gmol^{-1}$	445.99	441.14
Crystal size / mm	0.72 x 0.10 x 0.07	0.45 x 0.18 x 0.04
Crystal system	orthorhombic	monoclinic
Space group	Pbcn	C2/c
Unit cell dimensions		
a / Å	16.7781(8)	23.3770(12)
b / Å	17.5851(8)	12.7547(7)
c / Å	6.8233(3)	6.7212(3)
α / °	90	90
β / °	90	94.890(4)
γ / °	90	90
Volume / Å	2013.18(16)	1996.74(17)
Z	4	4
ρcalc. / g cm-1	1.471	1.468
μ / mm-1	1.116	1.003
F(000)	932.0	928.0
Temperature / K	120	120
Diffractometer		
Radiation	Mo Kα (λ = 0.71073)	Mo Kα (λ = 0.71073)
θ – range for data collection / °	2.316 to 32.465	3.072 to 32.709
Index ranges	-24 < h < 21	-35 < h < 33
	-22 < k < 26	-19 < k < 19
	-9 < l < 7	-9 < l < 10
Collected reflections	17977	19606
Independent reflections	3150	3317
Completeness	0.865	0.904
Rint	0.0600	0.0396
Rsigma	0.0334	0.0300
Data/ restraints/ parameters		
Goodness-of-fit on F^2	1.096	1.106
Final R1 [I ≥ 2σ(I)]	0.0573	0.0483
Final wR2 [I ≥ 2σ(I)]	0.1539	0.1458
Final R1 [alldata]	0.0756	0.0650
Final wR2 [alldata]	0.1674	0.1534

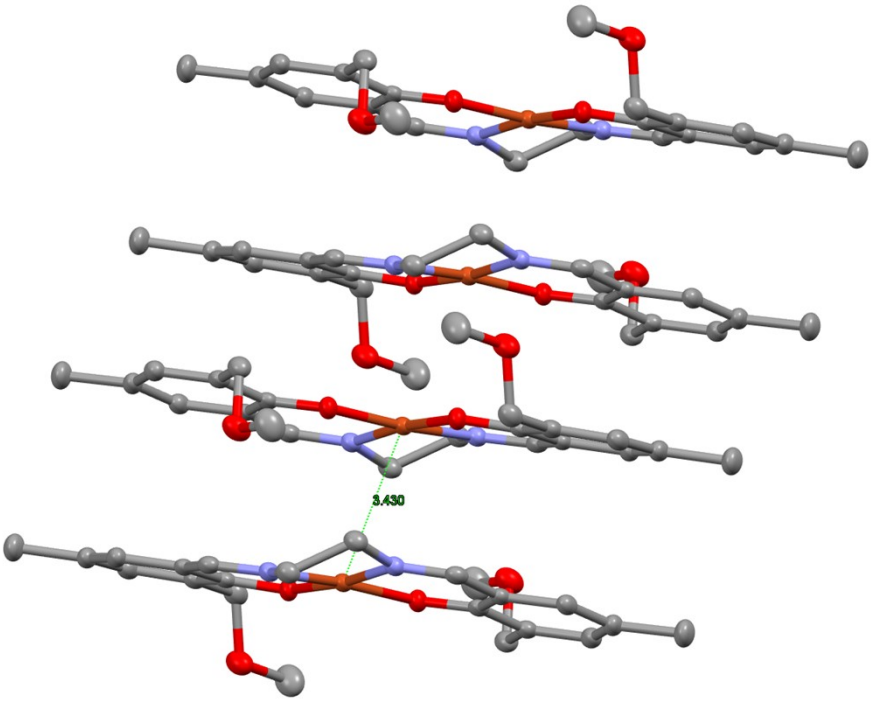

Figure S 9 Molecule stacking of $[Cu^{II}L^{Me}] \cdot 1.5\ H_2O$ (**C1**).

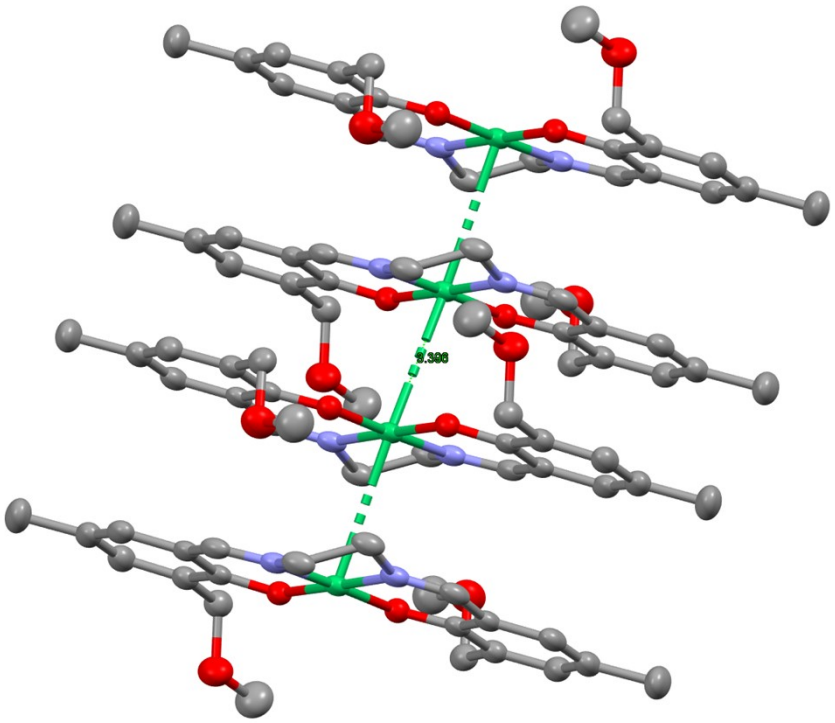

Figure S 10 Molecule stacking of $[Ni^{II}L^{Me}] \cdot 3\ H_2O$ (**C2**).

S4. Mass spectra

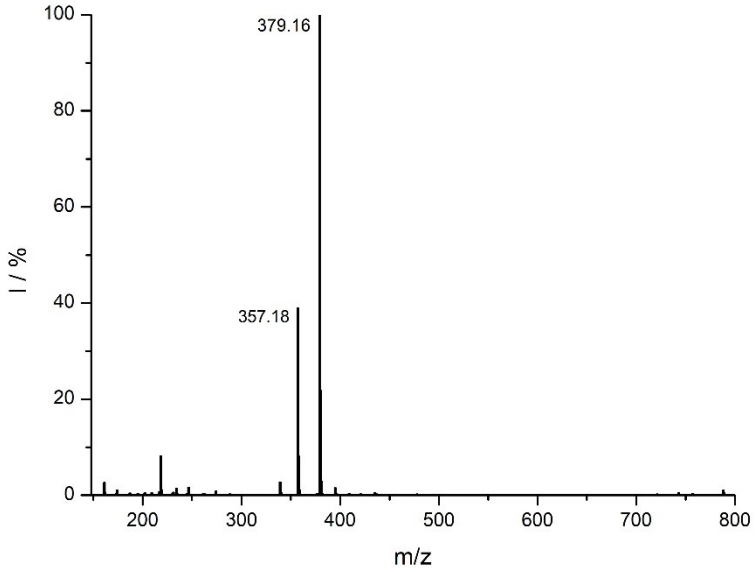

Figure S 11 ESI mass spectrum of ligand 6,6'-((1E,1'E)-(ethane-1,2-diylbis(azaneylylidene))bis(methaneylylidene)) bis(2-(hydroxymethyl)-4-methylphenol) (**H_4L)** with prominent peak at m/z 379.16, corresponding to the $[H_4L^+Na]^+$ ion.

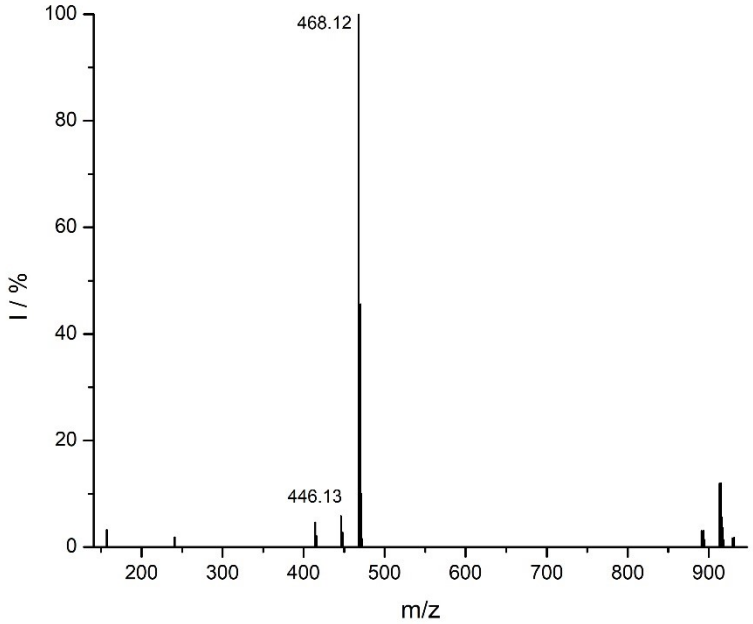

Figure S 12 ESI mass spectrum of copper complex $[Cu^{II}L^{Me}] \cdot 1.5\ H_2O$ (**C1**) with prominent peak at m/z 468.12, corresponding to the $[C1^+Na]^+$ ion.

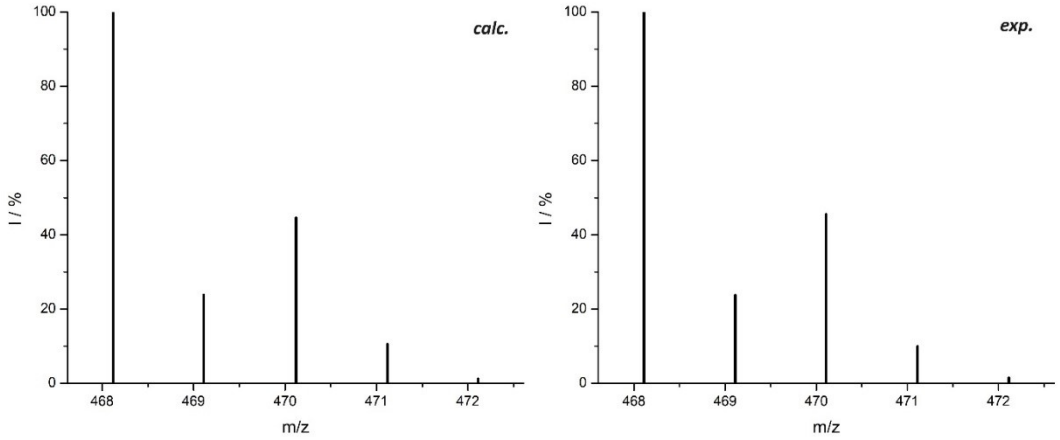

Figure S 13 Isotopic pattern of ESI mass spectra of copper complex $[Cu^{II}L^{Me}] \cdot 1.5\ H_2O$ (**C1**): predicted (left) and measured (right).

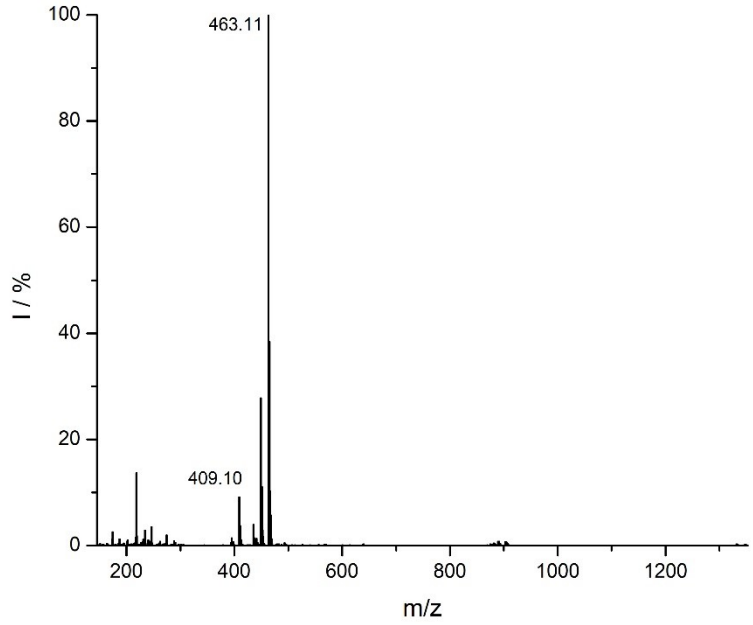

Figure S 14 ESI mass spectrum of nickel complex $[Ni^{II}L^{Me}] \cdot 3\ H_2O$ (**C2**) with prominent peak at m/z 463.11, corresponding to the $[C2^{+}Na]^{+}$ ion.

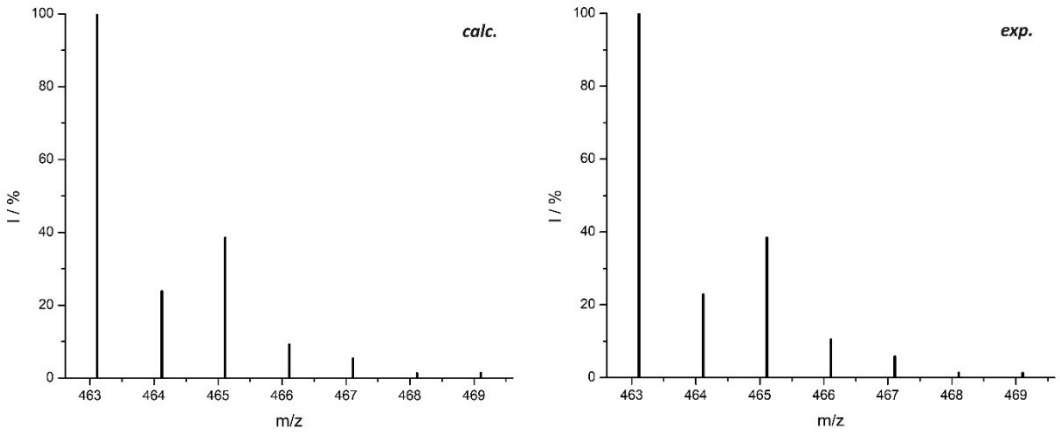

Figure S 15 Isotopic pattern of ESI mass spectra of copper complex $[Ni^{II}L^{Me}] \cdot 3\ H_2O$ (**C2**): predicted (left) and measured (right).

S5. Magnetic measurements

The EPR spectrum of the copper(II) complex **C1** was measured in solid state at room temperature and the data was analysed and fitted using the PHI software developed by the Chilton Group.[1] The resulting g-tensor values were g_1 = 2.063, g_2 = 2.041, and g_3 = 2.166, which follow the characteristic trend of $g_{II} > g_{\perp} > g_e$ (2.0023). This pattern is consistent with the square planar symmetry of the complex, with the unpaired ground-state electron located in the d_{x2-y2} orbital of the Cu(II) center.[2]

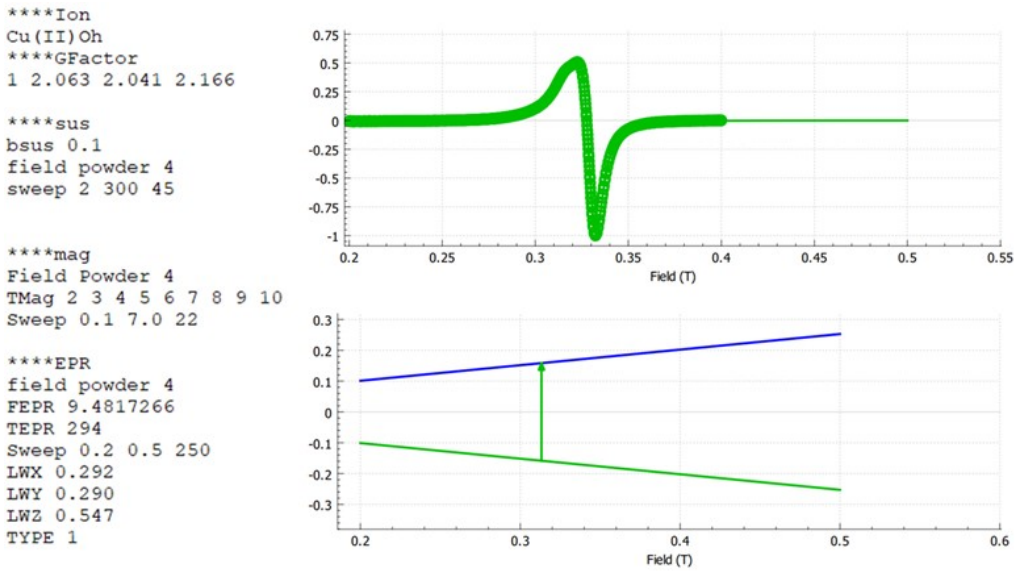

Figure S 16 EPR spectrum of $[Cu^{II}L^{Me}] \cdot 1.5\ H_2O$ (**C1**) (solid) measured at room temperature.

The magnetic properties of the copper(II) complex **C1** were studied by dc susceptibility measurements between 300 and 2 K. The data was plotted and fitted using PHI Software by The Chilton Group[1], as displayed in **Figure17**. The Cu(II) complex in powder form yielded a room-temperature magnetic susceptibility χT value of 0.39 ($cm^3\ mol^{-1}\ K$) and an isotropic g-value of 2.026. The theoretical χT for a spin-only S = 1/2 system with the experimentally determined g = 2.026 can be calculated from Curie's law[3] to 0.385 ($cm^3\ mol^{-1}\ K$), which is in good agreement with the measured value. These results are therefore consistent with the presence of a single unpaired electron (S = 1/2) per Cu(II) center, as expected for a d^9 configuration.

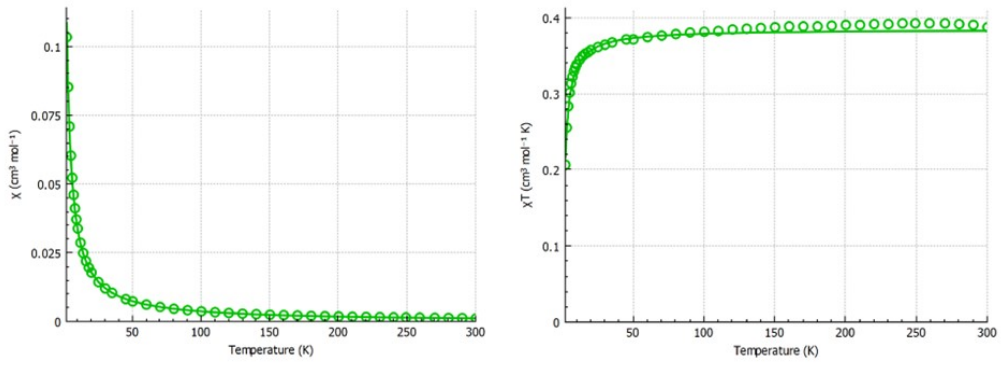

Figure S 17 Measured and fitted χ *vs*. temperture T curve (left) and magnetic susceptibility χT *vs*. temperature T (right) of $[Cu^{II}L^{Me}] \cdot 1.5\ H_2O$ (**C1**) (solid, powder).

Compared to the anisotropic values given by the EPR spectrum, only one isotropic value could be calculated from the magnetic data. This is because the magnetic data was measured from a powder sample, which can only provide powder-averaged g-value from bulk susceptibility.

S6. UV-VIS spectra

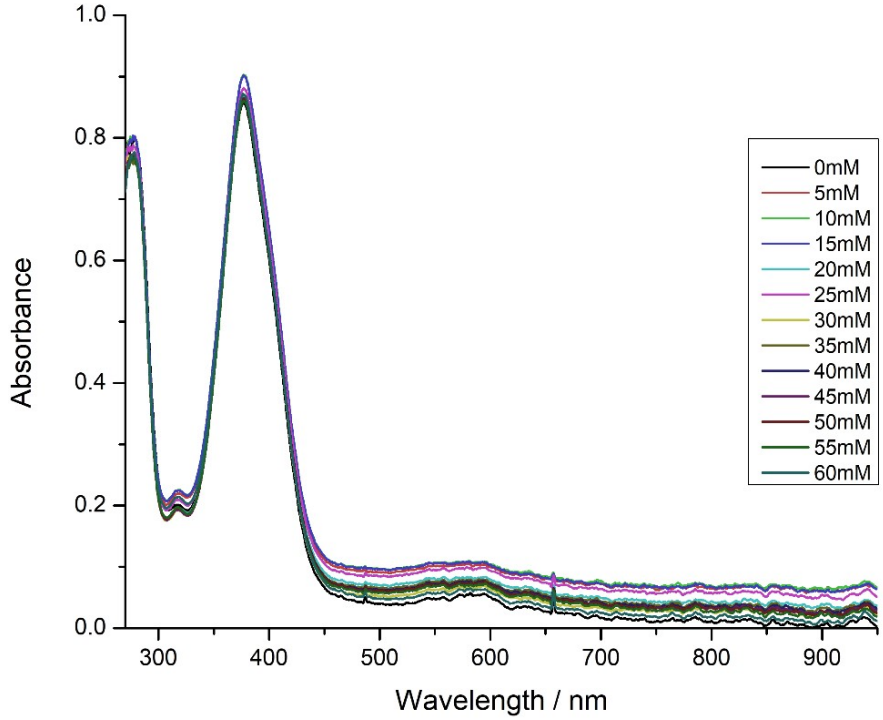

Figure S 18 Acid stability test conducted on $[Cu^{II}L^{Me}] \cdot 1.5\ H_2O$ (**C1**) in dmf with acetic acid at various concentrations.

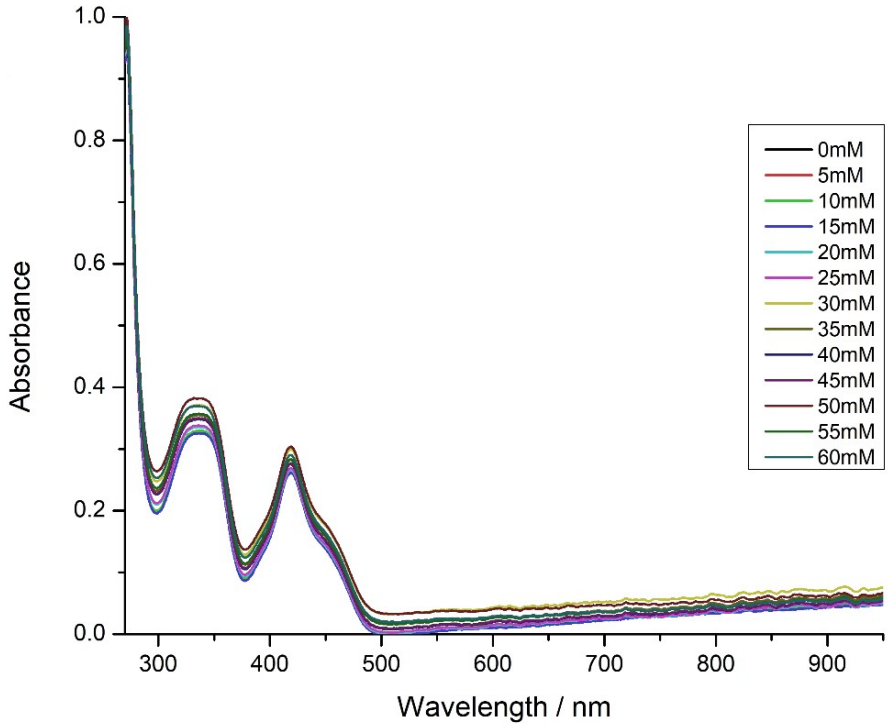

Figure S 19 Acid stability test conducted on $[Ni^{II}L^{Me}] \cdot 3\ H_2O$ (**C2**) in dmf with acetic acid at various concentrations.

S7. Cyclic voltammetry

Cyclic voltammetry measurements including scan rate study were performed on complexes **C1** and **C2**, as well as the ligand $\mathbf{LH_4}$ (**Figure S 20- S 22**). As seen in **Figure S 22** the ligand undergoes a $\mathbf{LH_4^0}$ to $\mathbf{LH_4^-}$ reduction at about -1.5 V *vs* Fc/Fc^+. The reversed oxidation process shows dependance to the scan rate with a close to zero anodic peak current at a low scan rate of 100 mV/s. This is typical for EC mechanisms and suggests a chemical transformation of the reduced ligand $\mathbf{LH_4^-}$ to $\mathbf{LH_4^*}$. Further, the scan rate dependent anodic peak close to -0.3 V *vs* Fc/Fc^+ indicates a second chemical transformation from $\mathbf{LH_4^*}$ to $\mathbf{LH_4^{**}}$ shortly after the first and suggests that at slower scan rate all $\mathbf{LH_4^*}$ has chemically transformed into $\mathbf{LH_4^{**}}$ and can therefore not be oxidized to $\mathbf{LH_4^{*+}}$ as seen for faster scan rates.

The CV and scan rate study of the copper complex **C1,** shown in **Figure S 20**, reveals similar behavior to that of the ligand $\mathbf{LH_4}$. The cathodic peak around – 1.7 V can be attributed to the $\mathbf{LH_4^0}$ to $\mathbf{LH_4^-}$ reduction process, followed by a scan rate dependent anodic process, suggesting a ligand centered chemical transformation. A semi-reversible, copper-centered redox process ($\mathbf{Cu^{II/I}}$) is observed just around -1.3 V. The reversed oxidation process is followed by a stripping peak at -0.3 V *vs* Fc/Fc^+, indicating the chemical decomposition of the complex.

The Ni(II) complex **C2** as shown in **Figure S 21**, undergoes a semi reversible oxidation from $\mathbf{Ni^{II}}$ to $\mathbf{Ni^{III}}$, as well as a semi reversible reduction from $\mathbf{Ni^{II}}$ to $\mathbf{Ni^{I}}$.[4]

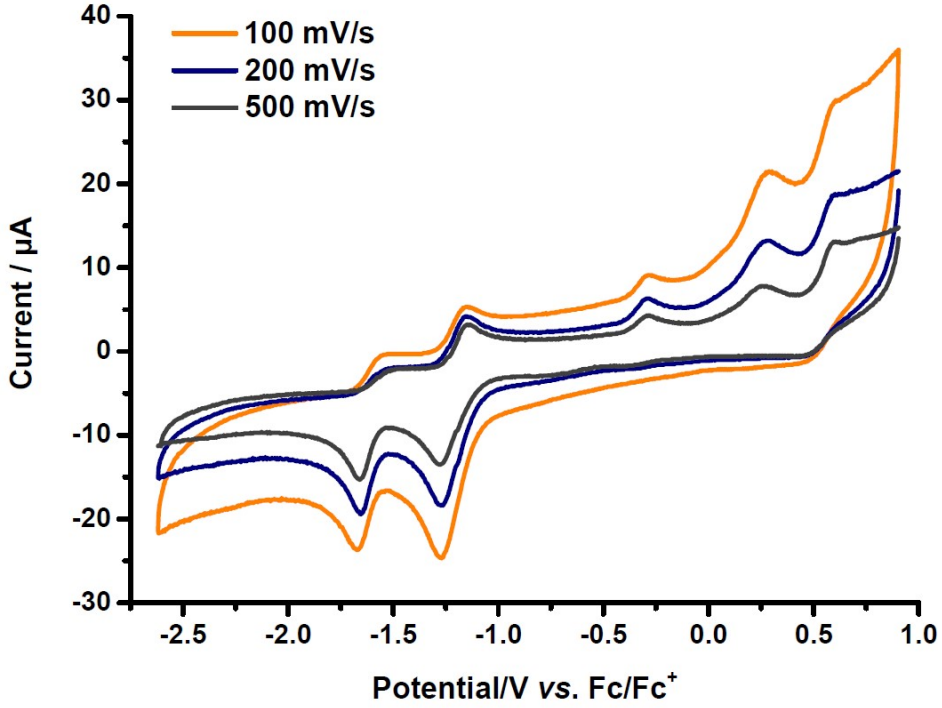

Figure S 20 Scan rate study of $[Cu^{II}L^{Me}] \cdot 1.5\ H_2O$ (**C1**) at (100, 200 and 500) mV/s.

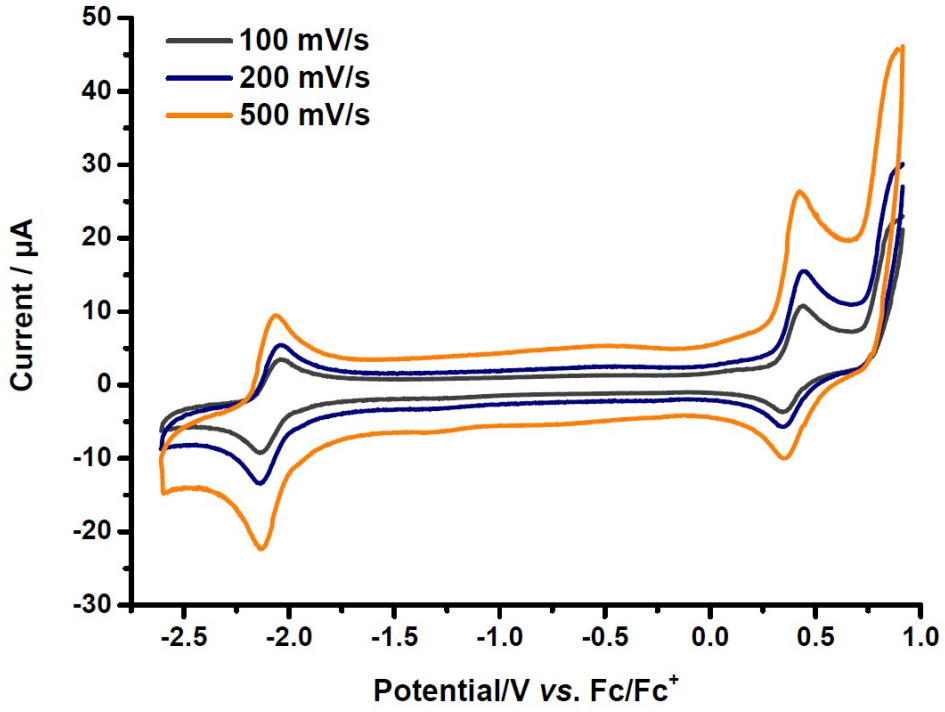

Figure S 21 Scan rate study of $[Ni^{II}L^{Me}] \cdot 3\ H_2O$ (**C2**) at (100, 200 and 500) mV/s.

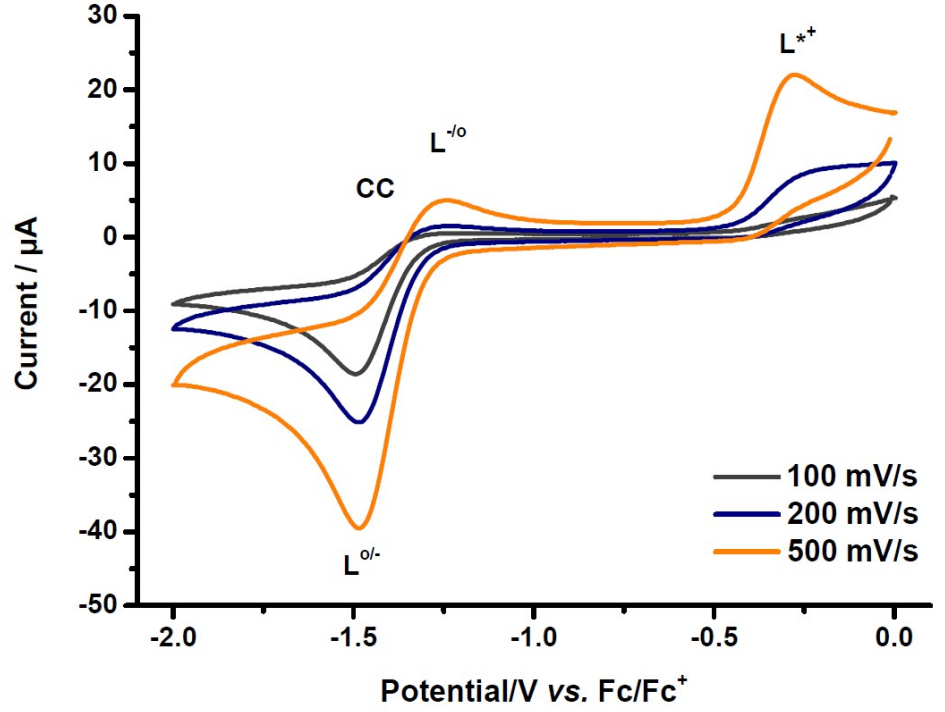

Figure S 22 CV measurement of ligand 6,6'-((1E,1'E)-(ethane-1,2-diylbis(azaneylylidene))bis(methaneylylidene))bis(2-(hydroxy-methyl)-4-methylphenol) (**H_4L**) with scan rate study and suggested mechanism.

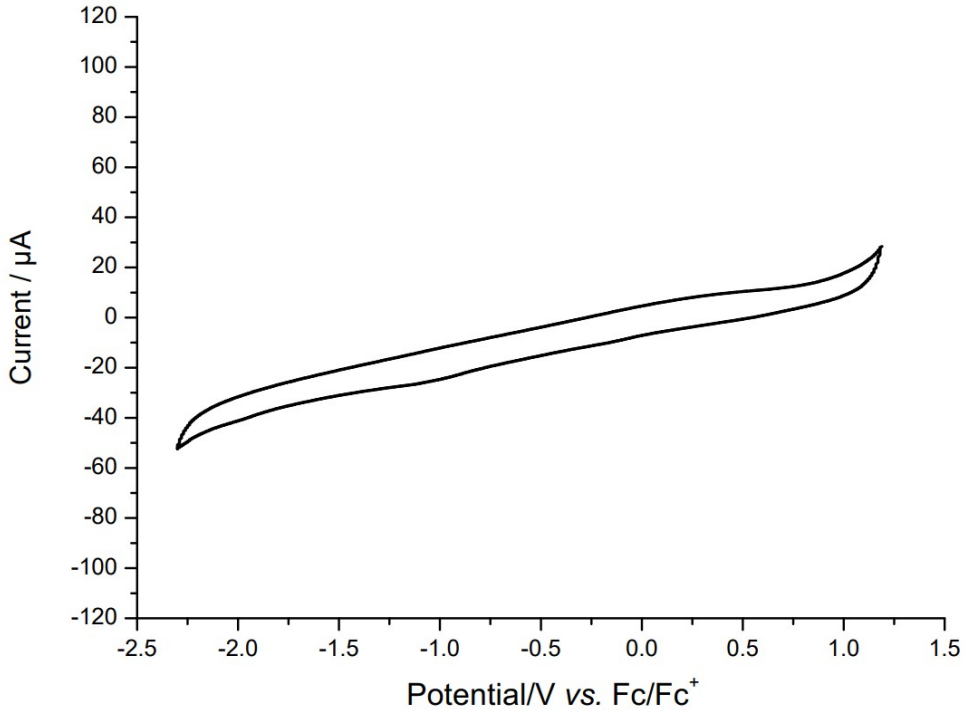

Figure S 23 Full range CV of Acetic Acid in DMF at a scan rate of 200 mv/s.

S8. Electrocatalysis

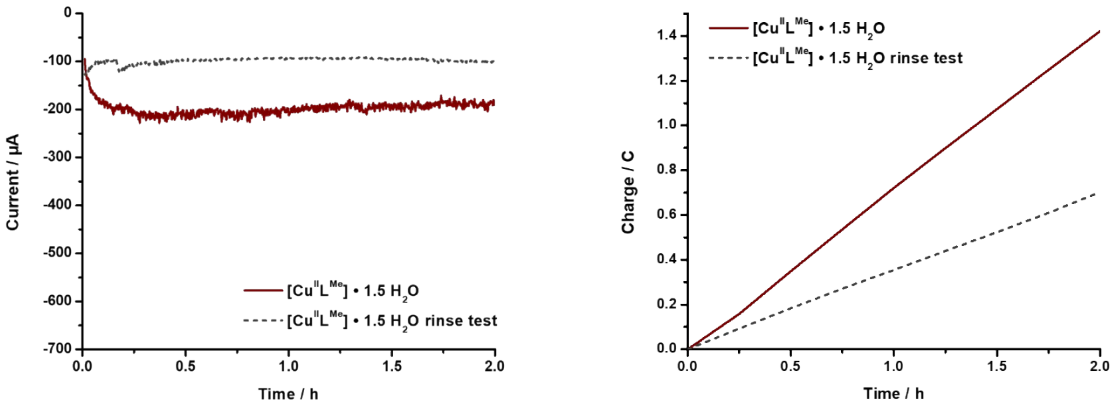

Figure S 24 2 hours bulk electrolysis of copper complex $[Cu^{II}L^{Me}] \cdot 1.5\ H_2O$ (**C1**) (0.5 mM in DMF with 60 mM acetic acid) at constant potential of -1.95 V with glassy carbon electrode (⌀ 3 mm) and rinse test (right) and accumulated charge against time (left).

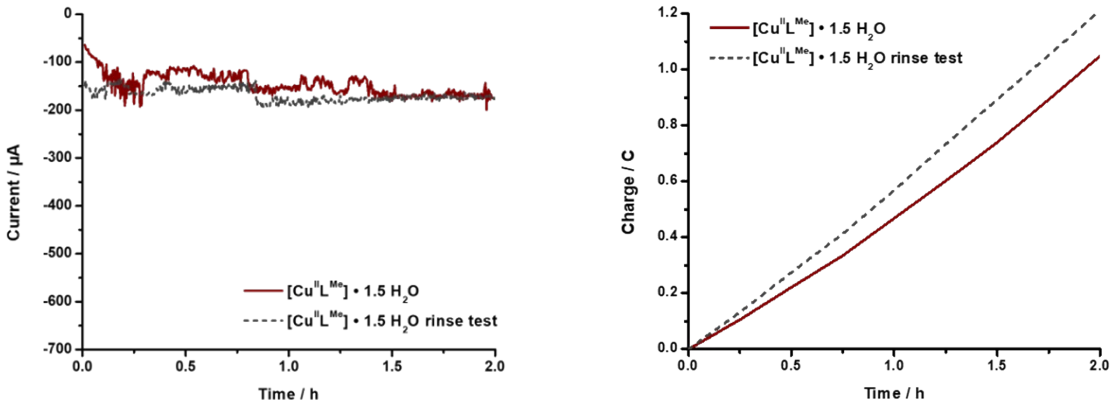

Figure S 25 2 hours bulk electrolysis of copper complex $[Cu^{II}L^{Me}] \cdot 1.5\ H_2O$ (**C1**) (0.5 mM in DMF with 60 mM acetic acid) at constant potential of -2.05 V with glassy carbon electrode (⌀ 3 mm) and rinse test (left) and accumulated charge against time (right).

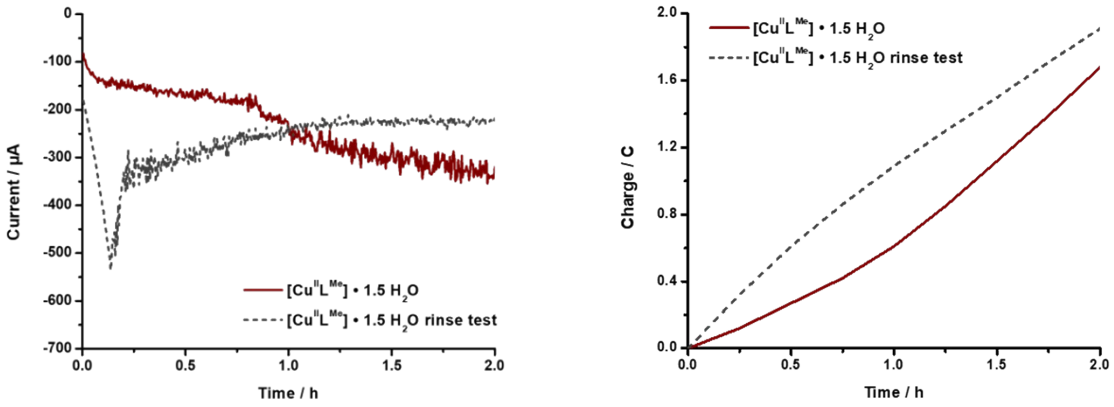

Figure S 26 2 hours bulk electrolysis of copper complex $[Cu^{II}L^{Me}] \cdot 1.5\ H_2O$ (**C1**) (0.5 mM in DMF with 60 mM acetic acid) at constant potential of -2.15 V with glassy carbon electrode (⌀ 3 mm) and rinse test (left) and accumulated charge against time (right).

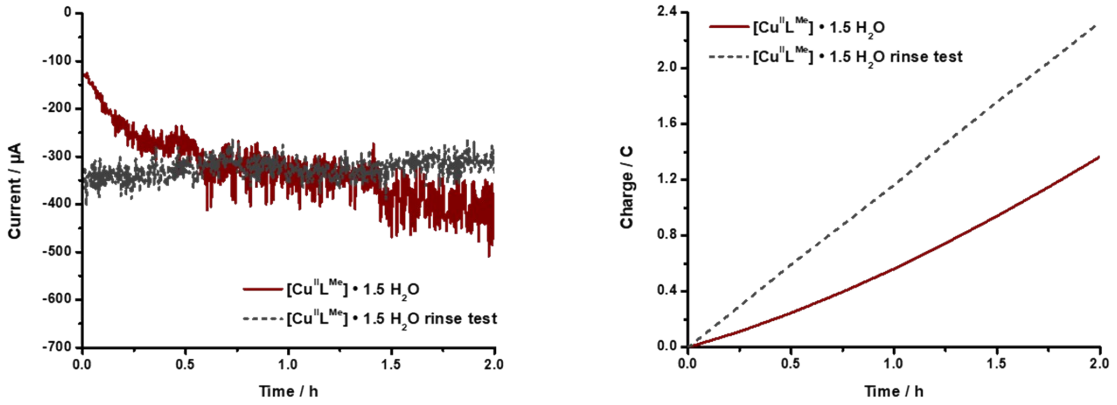

Figure S 27 2 hours bulk electrolysis of copper complex [Cu^{II}L^{Me}] · 1.5 H_2O (**C1**) (0.5 mM in DMF with 60 mM acetic acid) at constant potential of -2.25 V with glassy carbon electrode (⌀ 3 mm) and rinse test (left) and accumulated charge against time (right).

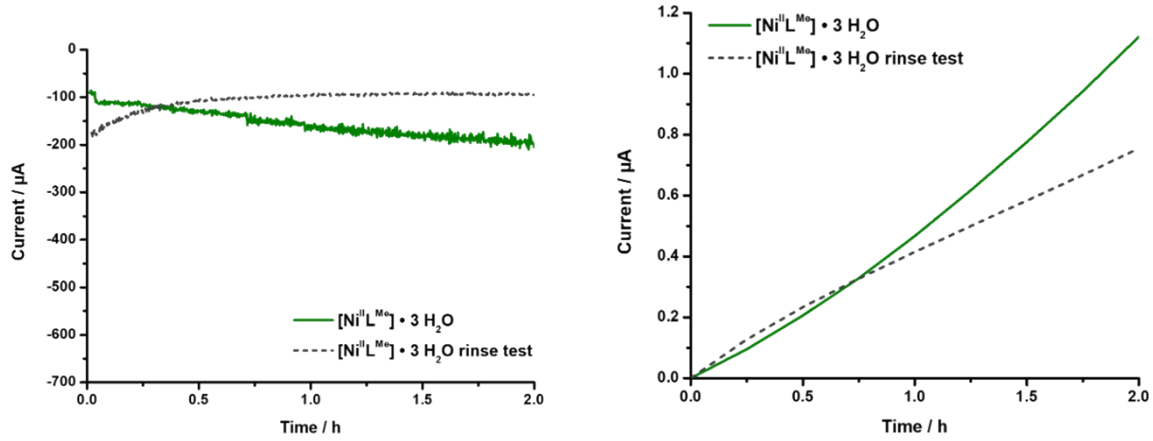

Figure S 28 2 hours bulk electrolysis of copper complex [Ni^{II}L^{Me}] · 3 H_2O (**C1**) (0.5 mM in DMF with 60 mM acetic acid) at constant potential of -2.05 V with glassy carbon electrode (⌀ 3 mm) and rinse test (left) and accumulated charge against time (right).

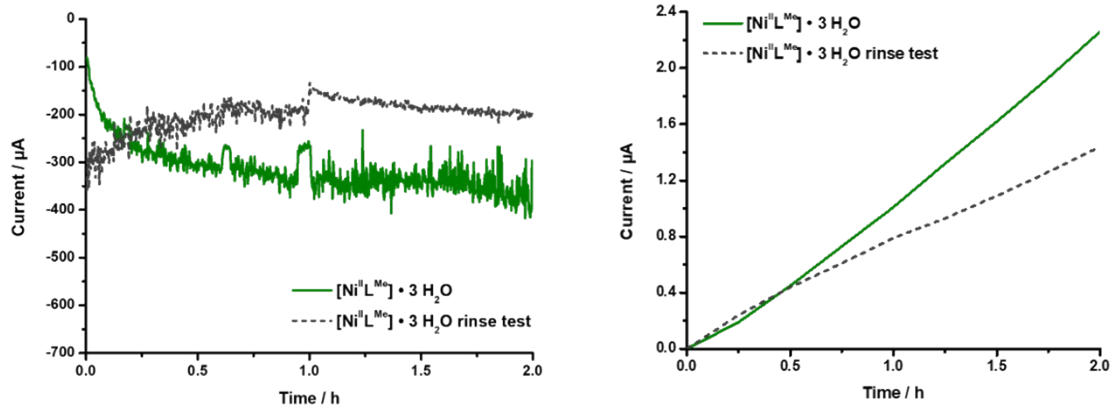

Figure S 29 2 hours bulk electrolysis of nickel complex [Ni^{II}L^{Me}] · 3 H_2O (**C2**) (0.5 mM in DMF with 60 mM acetic acid) at constant potential of -2.25 V with glassy carbon plate and rinse test.

S9. Gas chromatography

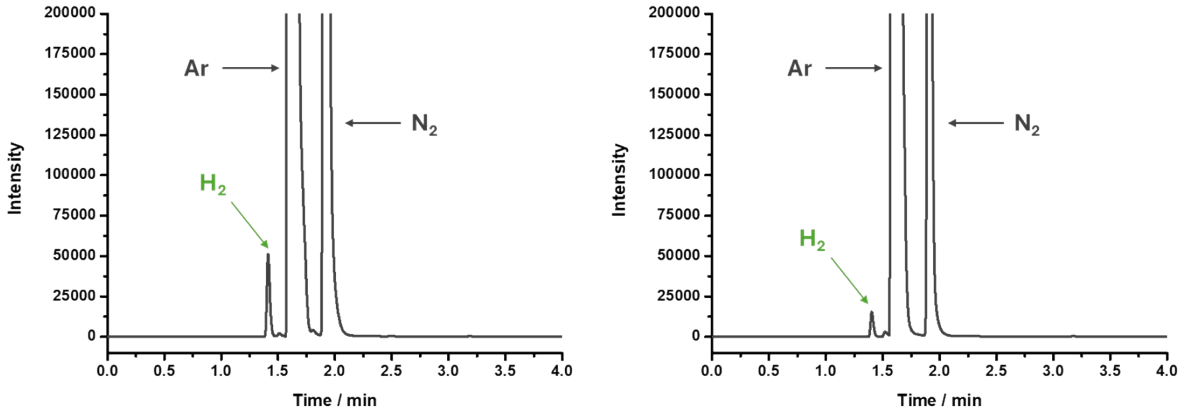

Figure S 30 Gas chromatogram of 100 µl air sample after 2 hours electrolysis of copper complex [$Cu^{II}L^{Me}$] · 1.5 H_2O (**C1**) (0.5 mM in DMF with 60 mM acetic acid) at constant potential of -1.95 V (left) and rinse test (right).

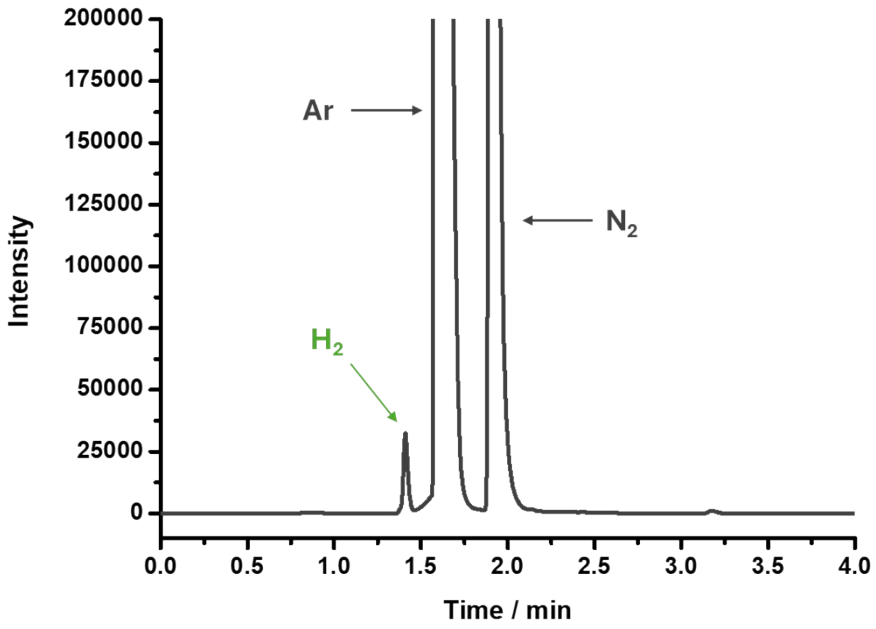

Figure S 31 Gas chromatogram of 100 µl air sample after 2 hours electrolysis of nickel complex [$Ni^{II}L^{Me}$] · 3 H_2O (**C2**) (0.5 mM in DMF with 60 mM acetic acid) at constant potential of -2.05 V.

Table S 2 Peak Table for GC measurement of 100 µl air sample after 2 hours electrolysis of copper complex $[Cu^{II}L^{Me}] \cdot 1.5\ H_2O$ (**C1**) (0.5 mM in DMF with 60 mM acetic acid) at constant potential of -1.95 V.

Peak#	R.Time	I.Time	F.Time	Area	Height	A/H	Conc.	Mark	ID#	Name	k'	Plate #	Plate Ht.	Tailing	Resolution	Sep. Factor	Area Ratio	Height Ratio	Conc. %	Norm Conc.
1	1.413	1.367	1.484	96283	50638	1.901	9.243		1	H2	0	13184	11.378	1.31	0	0	0	0	100	100
2	1.513	1.484	1.568	5486	2243	2.446	0	V			0.07	9422	15.92	0	1.782	0	0	0	0	0
3	1.622	1.568	1.871	26889497	7857477	3.422	0	SV	2	O2	0.148	4358	34.423	1.047	1.361	2.1	0	0	0	0
4	1.808	1.792	1.857	2123	1301	1.632	0	T			0.279	26126	5.741	1.599	2.596	1.89	0	0	0	0
5	1.915	1.871	2.604	6968506	3062779	2.275	0	SV	3	N2	0.355	17949	8.357	1.503	2.102	1.272	0	0	0	0

Table S 3 Compound Results for GC measurement of 100 µl air sample after 2 hours electrolysis of copper complex $[Cu^{II}L^{Me}] \cdot 1.5\ H_2O$ (**C1**) (0.5 mM in DMF with 60 mM acetic acid) at constant potential of -1.95 V.

ID#	Name	R.Time	Area	Height	Conc.	Curve	3rd	2nd	1st	Constant	Area Ratio	Height Ratio	Conc. %	Norm Conc.
1	H2	1.413	96283	50638	9.243	Linear	0.00E+00	0.00E+00	1.05E+04	-7.64E+02	0	0	100	100
2	O2	1.622	26889497	7857477	0	Linear	0.00E+00	0.00E+00	0.00E+00	0.00E+00	0	0	0	0
3	N2	1.915	6968506	3062779	0	Linear	0.00E+00	0.00E+00	0.00E+00	0.00E+00	0	0	0	0
4	CH4	0	0	0	0	Linear	0.00E+00	0.00E+00	9.43E+04	-9.93E+03	0	0	0	0
5	CO	0	0	0	0	Linear	0.00E+00	0.00E+00	4.65E+04	-6.44E+03	0	0	0	0

Table S 4 Peak Table for GC measurement of 100 µl air sample from rinse test after 2h electrolysis of copper complex $[Cu^{II}L^{Me}] \cdot 1.5\ H_2O$ (**C1**) (0.5 mM in DMF with 60 mM acetic acid) at constant potential of -1.95 V.

Peak#	R.Time	I.Time	F.Time	Area	Height	A/H	Conc.	Mark	ID#	Name	k'	Plate #	Plate Ht.	Tailing	Resolution	Sep. Factor	Area Ratio	Height Ratio	Conc. %	Norm Conc.
1	1.404	1.367	1.489	27920	15171	1.84	2.732		1	H2	0	14154	10.597	1.32	0	0	0	0	100	100
2	1.521	1.489	1.559	7286	3137	2.323	0	V			0.083	9282	16.161	0	2.12	0	0	0	0	0
3	1.612	1.559	1.862	26299998	7827908	3.36	0	V	2	O2	0.148	4551	32.957	1.049	1.143	1.775	0	0	0	0
4	1.908	1.862	2.455	2283156	1078104	2.118	0	SV	3	N2	0.358	20169	7.437	1.366	3.96	2.423	0	0	0	0

Table S 5 Compound Results for GC measurement of 100 µl air sample from rinse test after 2h electrolysis of copper complex $[Cu^{II}L^{Me}] \cdot 1.5\ H_2O$ (**C1**) (0.5 mM in DMF with 60 mM acetic acid) at constant potential of -1.95 V.

ID#	Name	R.Time	Area	Height	Conc.	Curve	3rd	2nd	1st	Constant	Area Ratio	Height Ratio	Conc. %	Norm Conc.
1	H2	1.404	27920	15171	2.732	Linear	0.00E+00	0.00E+00	1.05E+04	-7.64E+02	0	0	100	100
2	O2	1.612	26299998	7827908	0	Linear	0.00E+00	0.00E+00	0.00E+00	0.00E+00	0	0	0	0
3	N2	1.908	2283156	1078104	0	Linear	0.00E+00	0.00E+00	0.00E+00	0.00E+00	0	0	0	0
4	CH4	0	0	0	0	Linear	0.00E+00	0.00E+00	9.43E+04	-9.93E+03	0	0	0	0
5	CO	0	0	0	0	Linear	0.00E+00	0.00E+00	4.65E+04	-6.44E+03	0	0	0	0

Table S 6 Peak Table Peak Table for GC measurement of 100 µl air sample after 2 hours electrolysis of nickel complex $[Ni^{II}L^{Me}] \cdot 3\ H_2O$ (**C2**) (0.5 mM in DMF with 60 mM acetic acid) at constant potential of -1.95 V.

Peak#	R.Time	I.Time	F.Time	Area	Height	A/H	Conc.	Mark	ID#	Name	k'	Plate #	Plate Ht.	Tailing	Resolution	Sep. Factor	Area Ratio	Height Ratio	Conc. %	Norm Conc.
1	1.41	1.349	1.465	63291	31964	1.98	6.101		1	H2	0	13464	11.141	1.154	0	0	0	0	96.449	96.449
2	1.618	1.465	1.867	27464830	8003422	3.432	0	V	2	O2	0.147	4175	35.924	1.052	2.794	0	0	0	0	0
3	1.91	1.867	2.716	6640371	2816499	2.358	0	SV	3	N2	0.354	16813	8.921	1.584	3.668	2.404	0	0	0	0
4	3.176	3.113	3.36	4013	1132	3.543	0.225		5	CO	1.252	22055	6.801	1.672	17.525	3.534	0	0	3.551	3.551

Table S 7 Compound Results for GC measurement of 100 µl air sample after 2 hours electrolysis of nickel complex $[Ni^{II}L^{Me}] \cdot 3\ H_2O$ (**C2**) (0.5 mM in DMF with 60 mM acetic acid) at constant potential of -1.95 V.

ID#	Name	R.Time	Area	Height	Conc.	Curve	3rd	2nd	1st	Constant	Area Ratio	Height Ratio	Conc. %	Norm Conc.
1	H2	1.41	63291	31964	6.101	Linear	0.00E+00	0.00E+00	1.05E+04	-7.64E+02	0	0	96.449	96.449
2	O2	1.618	27464830	8003422	0	Linear	0.00E+00	0.00E+00	0.00E+00	0.00E+00	0	0	0	0
3	N2	1.91	6640371	2816499	0	Linear	0.00E+00	0.00E+00	0.00E+00	0.00E+00	0	0	0	0
4	CH4	0	0	0	0	Linear	0.00E+00	0.00E+00	9.43E+04	-9.93E+03	0	0	0	0
5	CO	3.176	4013	1132	0.225	Linear	0.00E+00	0.00E+00	4.65E+04	-6.44E+03	0	0	3.551	3.551

S10. SEM/EDX

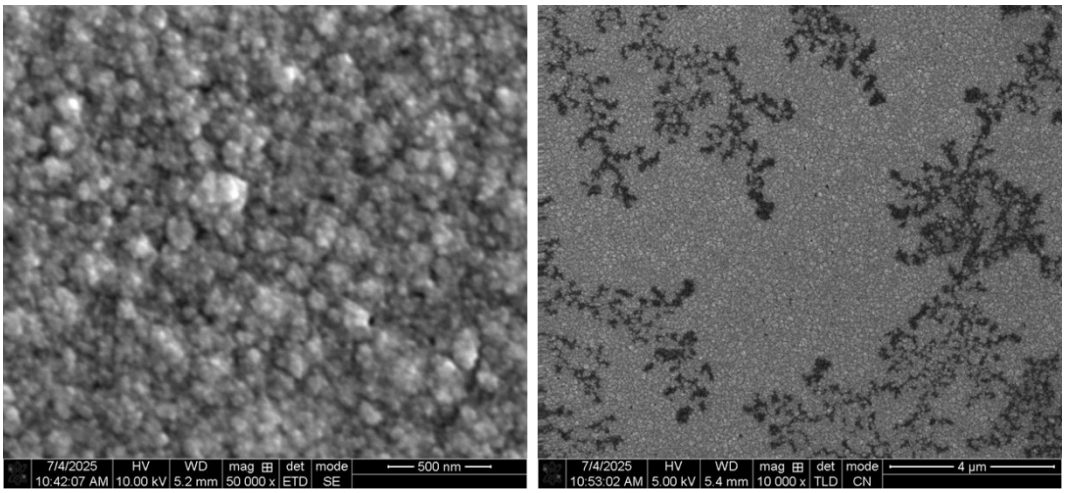

Figure S 32 SEM images of glassy carbon plate after 3 h bulk electrolysis at -1.9 v of copper complex $[Cu^{II}L^{Me}] \cdot 1.5\ H_2O$ (**C1**).

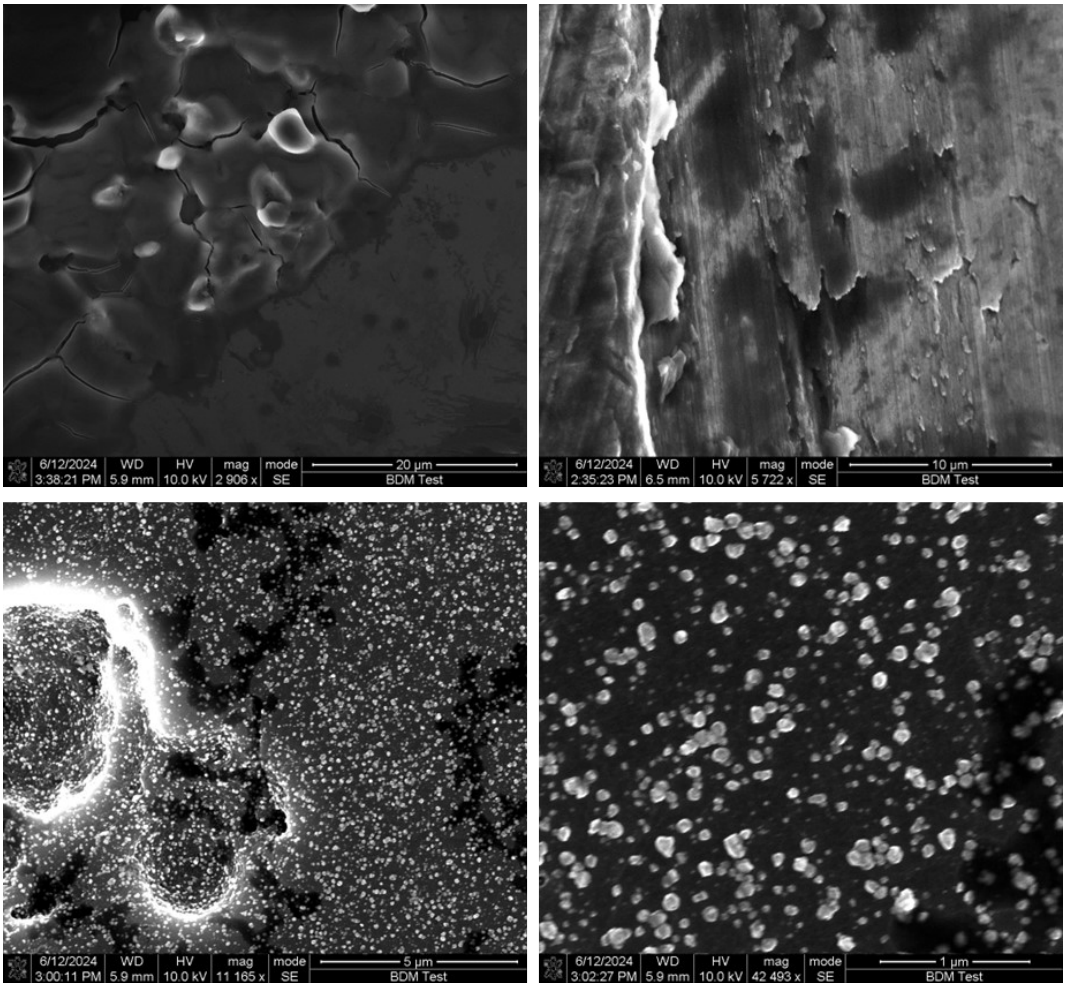

Figure S 33 SEM images of glassy carbon plate after 3 h bulk electrolysis at -1.9 V of nickel complex $[Ni^{II}L^{Me}] \cdot 3\ H_2O$ (**C2**).

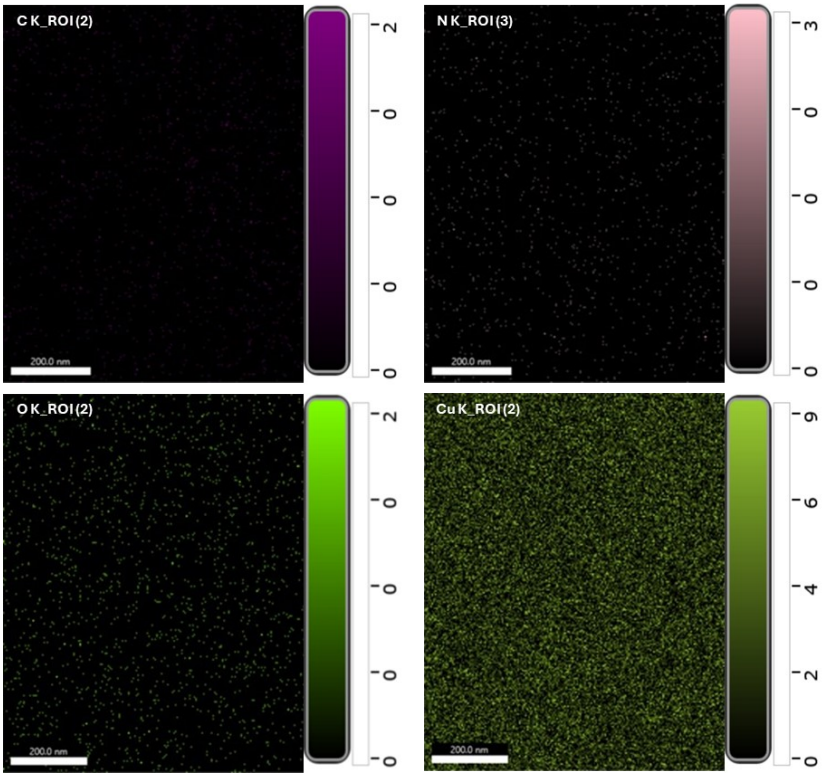

Figure S 34 Element detection of surface deposition on glassy carbon plate after 3 h bulk electrolysis of copper complex $[Cu^{II}L^{Me}] \cdot 1.5\ H_2O$ (**C1**) through EDX analysis: inside deposition.

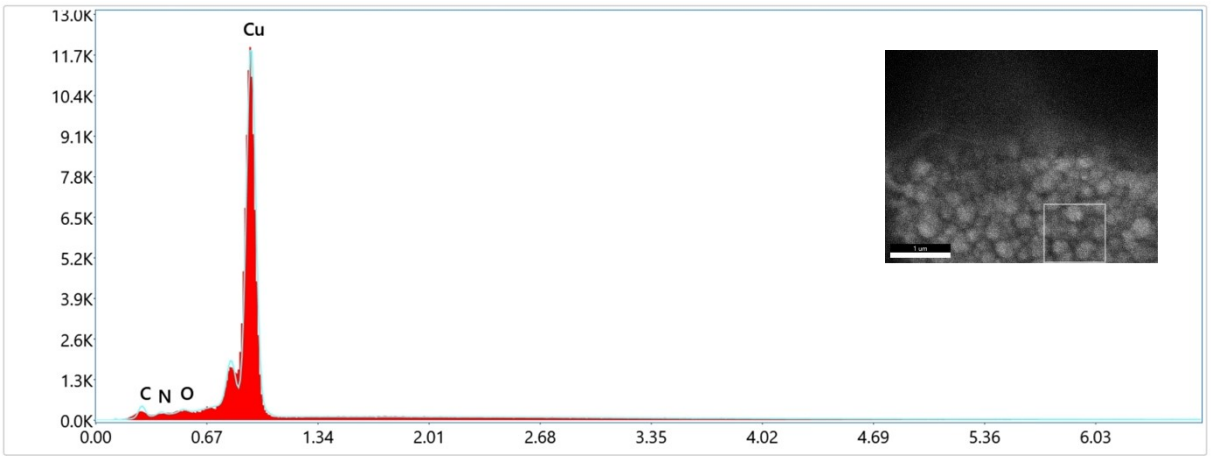

Figure S 35 EDX sum spectrum of glassy carbon plate inside surface deposition after 3 h bulk electrolysis of copper complex $[Cu^{II}L^{Me}] \cdot 1.5\ H_2O$ (**C1**) with live sample map.

Table S 8 Quantified results of EDX analysis of of glassy carbon plate inside surface deposition after 3 h bulk electrolysis of copper complex $[Cu^{II}L^{Me}] \cdot 1.5\ H_2O$ (**C1**), corresponding to sum spectrum in **Figure S34**.

Element	Weight %	MDL	Atomic %	Net Int.	Error %	R	A	F
C K	11.9	0.87	40.0	4.6	13.6	0.8058	0.1929	1.0000
N K	1.2	0.48	3.4	1.2	26.6	0.8155	0.2687	1.0000
O K	0.7	0.31	1.7	1.4	21.8	0.8236	0.4235	1.0000
Cu L	86.3	1.49	54.9	146.8	5.7	0.8414	0.6587	1.0000

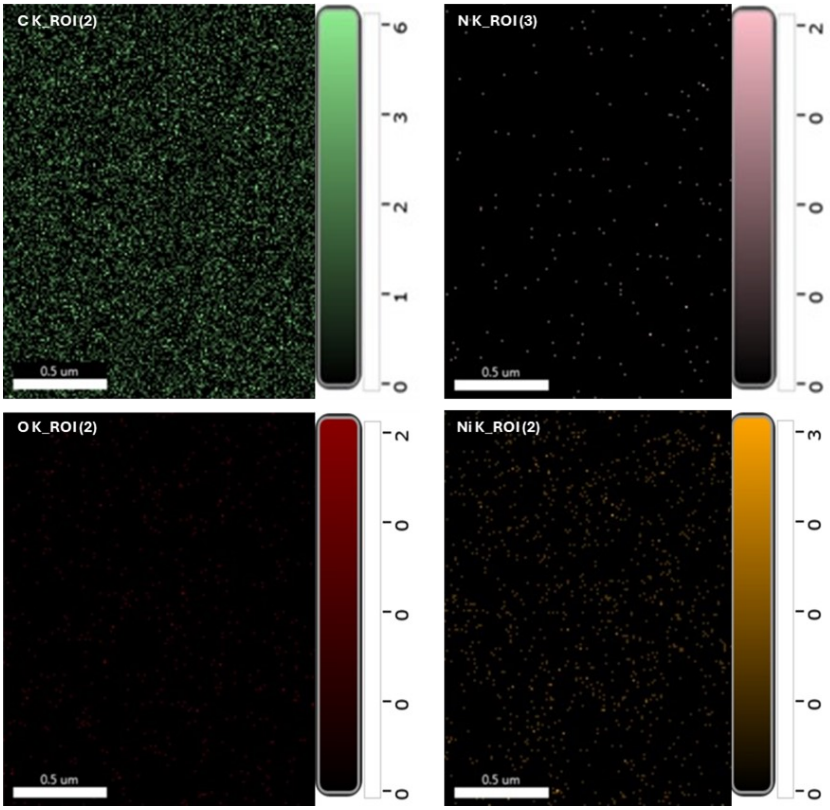

Figure S 36 Element detection of surface deposition on glassy carbon plate after 3 h bulk electrolysis of nickel complex [$Ni^{II}L^{Me}$] · 3 H_2O (**C2**) through EDX analysis: inside deposition.

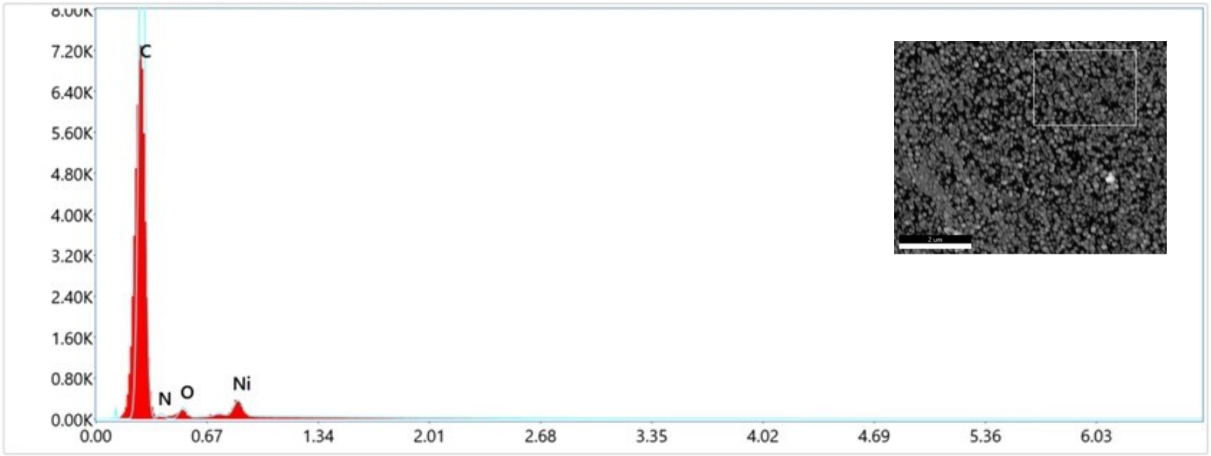

Figure S 37 EDX sum spectrum of glassy carbon plate inside surface deposition after 3 h bulk electrolysis at -1.9 V of nickel complex [$Ni^{II}L^{Me}$] · 3 H_2O (**C2**) with live sample map.

Table S 9 Quantified results of EDX analysis of glassy carbon plate inside surface deposition after 3 h bulk electrolysis of nickel complex [$Ni^{II}L^{Me}$] · 3 H_2O (**C2**), corresponding to sum spectrum in **Figure S36**.

Element	Weight %	MDL	Atomic %	Net Int.	Error %	R	A	F
C K	93.1	0.03	95.4	178.0	6.2	0.9456	0.5938	1.0000
N K	2.9	0.07	2.5	1.7	16.2	0.9502	0.1013	1.0000
O K	2.2	0.13	1.7	3.8	14.2	0.9539	0.2212	1.0000
Ni L	1.8	0.27	0.4	4.5	9.6	0.9602	0.5770	1.0000

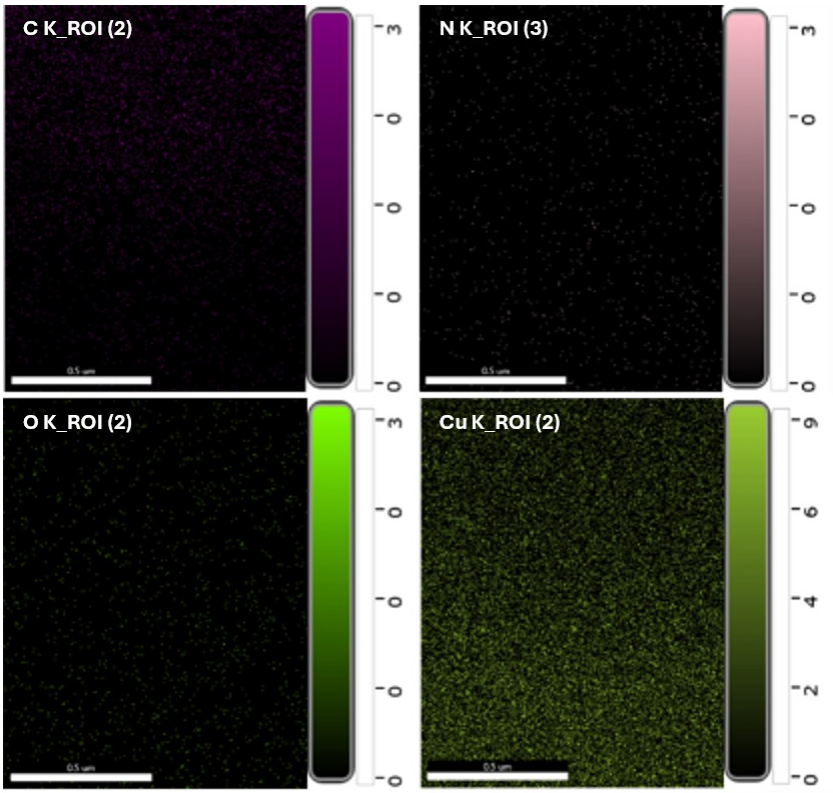

Figure S 38 Element detection of surface deposition on glassy carbon plate after 3 h bulk electrolysis of copper complex $[Cu^{II}L^{Me}] \cdot 1.5\ H_2O$ (**C1**) through EDX analysis: edge of deposition.

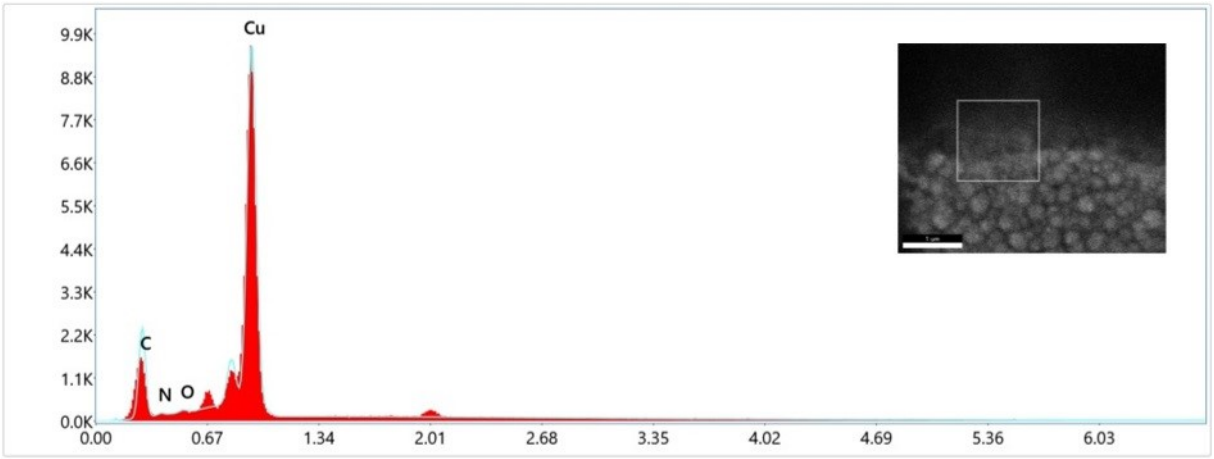

Figure S 39 EDX sum spectrum of edge of the deposited area on glassy carbon plate after 3 h bulk electrolysis of copper complex $[Cu^{II}L^{Me}] \cdot 1.5\ H_2O$ (**C1**) with live sample map.

Table S 10 Quantified results of EDX analysis of edge of the deposited area on glassy carbon plate after 3 h bulk electrolysis of copper complex $[Cu^{II}L^{Me}] \cdot 1.5\ H_2O$ (**C1**), corresponding to sum spectrum in **Figure S38**.

Element	Weight %	MDL	Atomic %	Net Int.	Error %	R	A	F
C K	42.8	0.51	78.7	27.5	10.2	0.8596	0.2674	1.0000
N K	0.8	0.57	1.3	0.6	43.1	0.8683	0.1763	1.0000
O K	0.4	0.32	0.5	0.8	49.0	0.8755	0.3315	1.0000
Cu L	56.0	1.08	19.5	113.6	5.8	0.8907	0.6516	1.0000

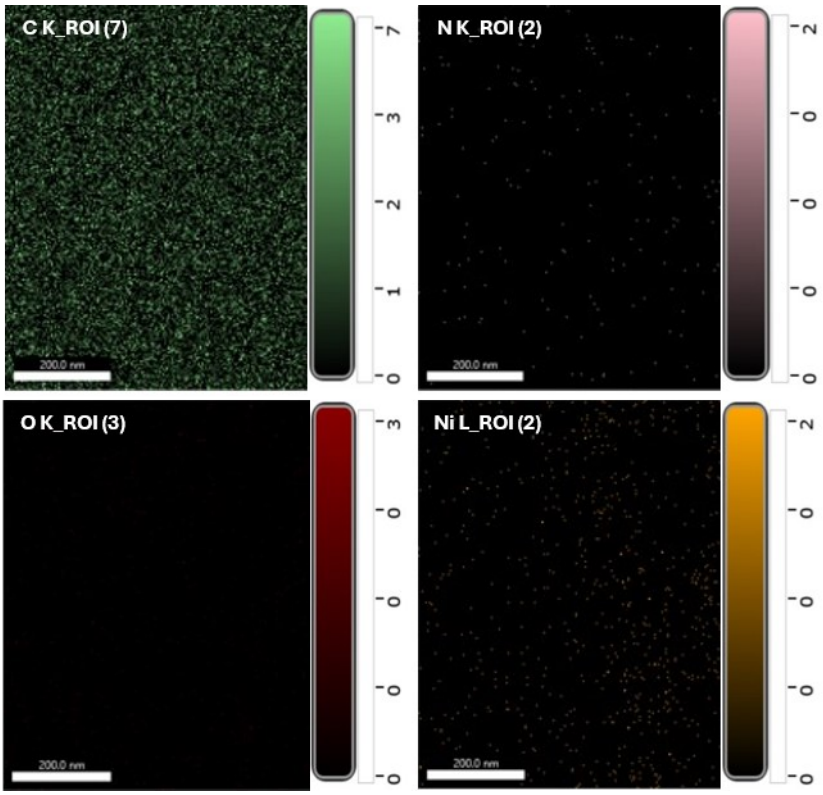

Figure S 40 Element detection of surface deposition on glassy carbon plate after 3 h bulk electrolysis of nickel complex $[Ni^{II}L^{Me}] \cdot 3\ H_2O$ (**C2**) through EDX analysis: edge of deposition.

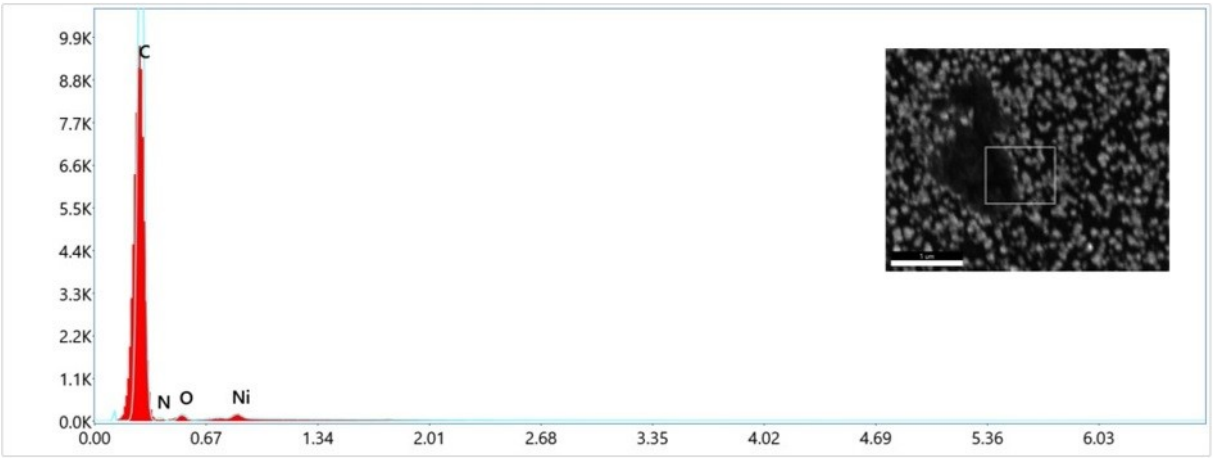

Figure S 41 EDX sum spectrum of edge of the deposited area on glassy carbon plate after 3 h bulk electrolysis of nickel complex $[Ni^{II}L^{Me}] \cdot 3\ H_2O$ (**C2**) with live sample map.

Table S 11 Quantified results of EDX analysis of edge of the deposited area on glassy carbon plate after 3 h bulk electrolysis of copper complex $[Ni^{II}L^{Me}] \cdot 3\ H_2O$ (**C2**), corresponding to sum spectrum in **Figure S40**.

Element	Weight %	MDL	Atomic %	Net Int.	Error %	R	A	F
C K	95.8	0.03	96.9	212.4	6.0	0.9476	0.6127	1.0000
N K	2.1	0.04	1.9	1.4	16.6	0.9521	0.0987	1.0000
O K	1.5	0.10	1.1	2.8	14.8	0.9557	0.2186	1.0000
Ni L	0.6	0.17	0.1	1.6	15.1	0.9618	0.5809	1.0000

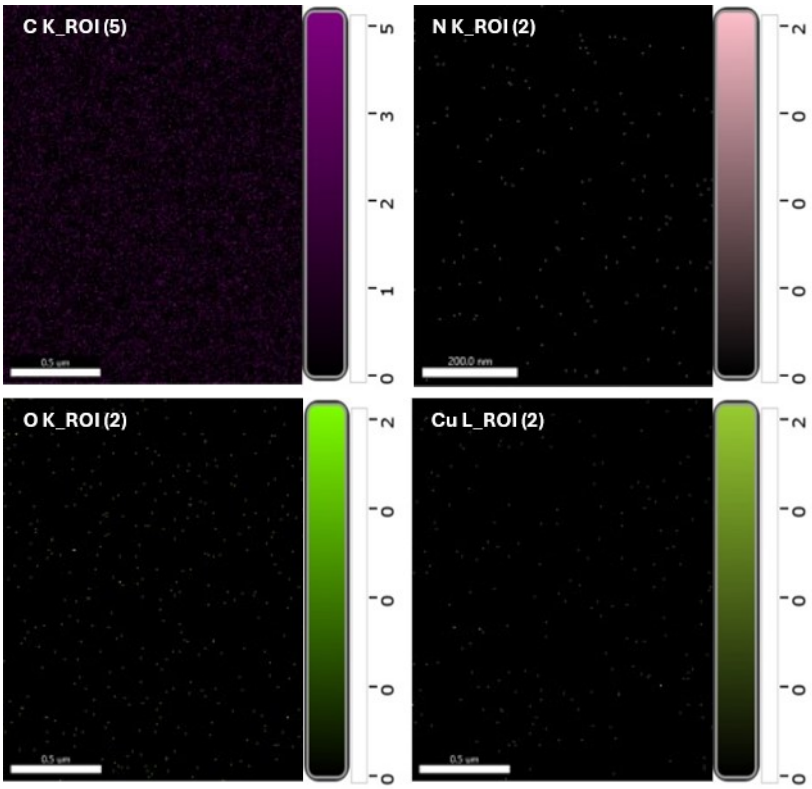

Figure S 42 Element detection of surface deposition on glassy carbon plate after 3 h bulk electrolysis of nickel complex [$Ni^{II}L^{Me}$] · 3 H_2O (**C2**) through EDX analysis: bare plate.

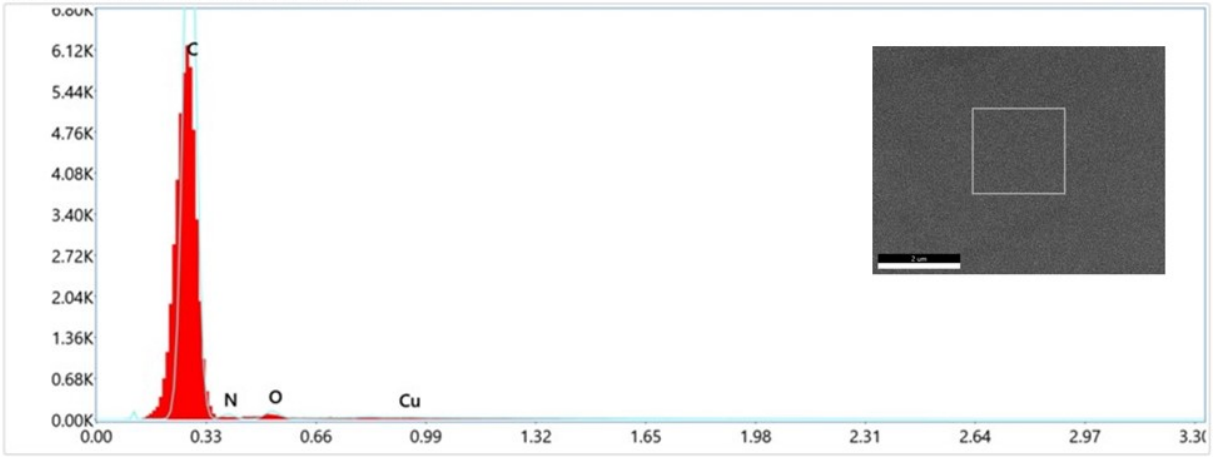

Figure S 43 EDX sum spectrum of a bare glassy carbon plate after 3 h bulk electrolysis of nickel complex [$Cu^{II}L^{Me}$] · 1.5 H_2O (**C1**) with live sample map.

Table S 12 Quantified results of EDX analysis of a bare glassy carbon plate after 3 h bulk electrolysis of copper complex [$Cu^{II}L^{Me}$] · 1.5 H_2O (**C1**), corresponding to sum spectrum in **Figure S42**.

Element	Weight %	MDL	Atomic %	Net Int.	Error %	R	A	F
C K	97.6	0.04	98.1	117.8	5.4	0.9542	0.8650	1.0000
N K	1.3	0.03	1.1	1.2	15.6	0.9592	0.3658	1.0000
O K	1.0	0.08	0.8	1.8	13.5	0.9631	0.5800	1.0000
Cu L	0.1	0.21	0.0	0.1	64.7	0.9714	0.8831	1.0000

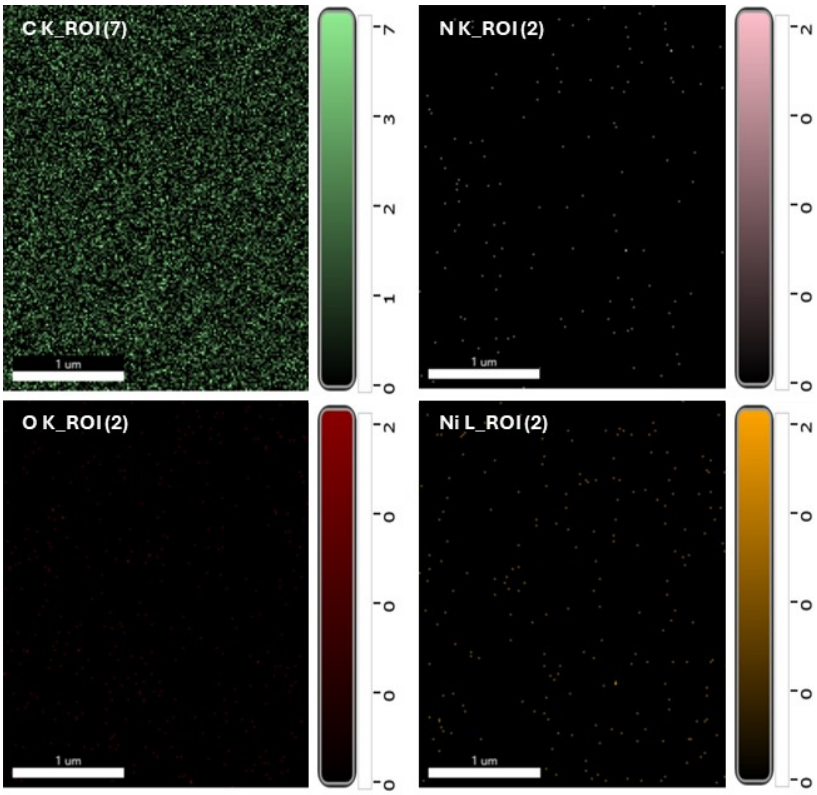

Figure S 44 Element detection of surface deposition on glassy carbon plate after 3 h bulk electrolysis of nickel complex [$Ni^{II}L^{Me}$] · 3 H_2O (**C2**) through EDX analysis: bare plate.

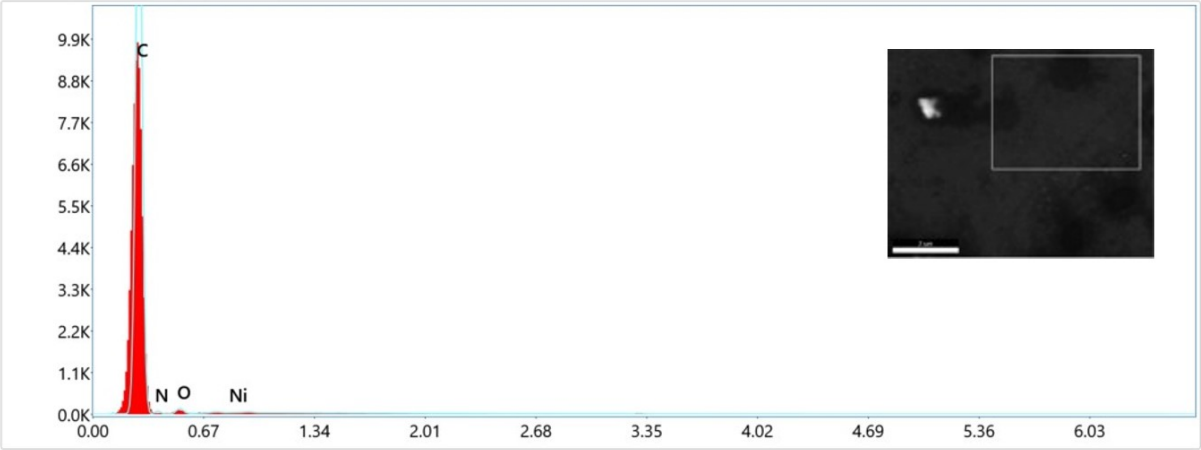

Figure S 45 EDX sum spectrum of a bare glassy carbon plate after 3 h bulk electrolysis of nickel complex [$Ni^{II}L^{Me}$] · 3 H_2O (**C2**) with live sample map.

Table S 13 Quantified results of EDX analysis of a bare glassy carbon plate after 3 h bulk electrolysis of nickel complex [$Ni^{II}L^{Me}$] · 3 H_2O (**C2**), corresponding to sum spectrum in **Figure S44**.

Element	Weight %	MDL	Atomic %	Net Int.	Error %	R	A	F
C K	97.0	0.03	97.6	230.5	5.9	0.9485	0.6218	1.0000
N K	1.8	0.04	1.5	1.2	17.3	0.9529	0.0976	1.0000
O K	1.2	0.09	0.9	2.4	15.5	0.9564	0.2177	1.0000
Ni L	0.0	0.13	0.0	0.0	46.8	0.9625	0.5827	1.0000

S11. DLS

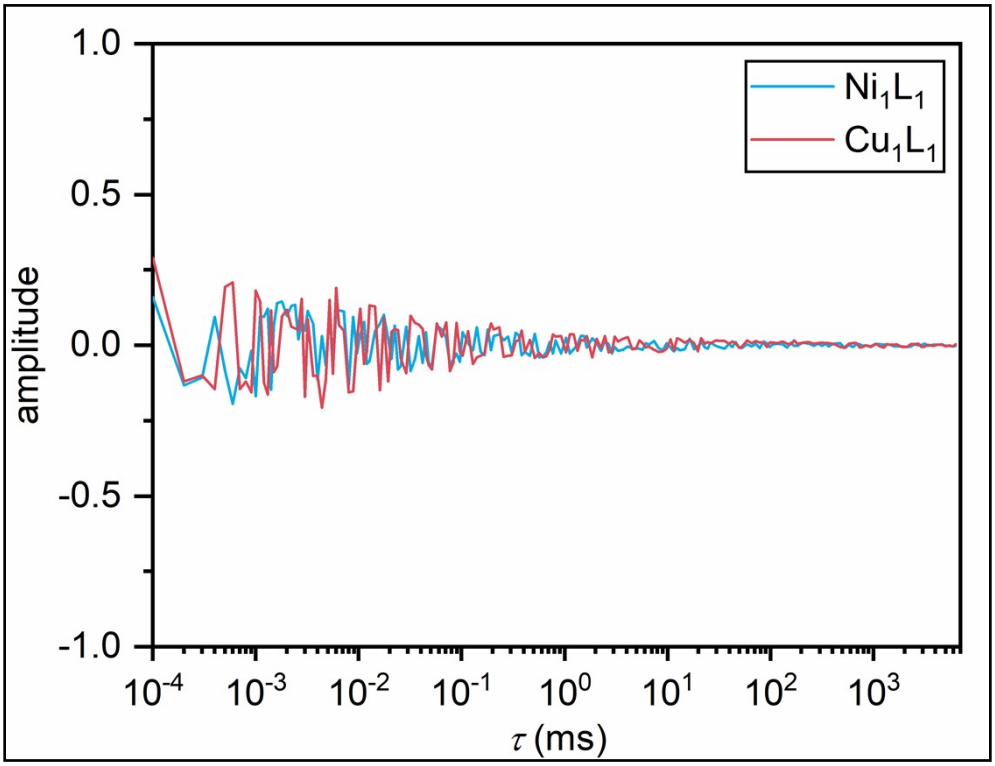

Figure S 46 Autocorrelation functions measured at 30° for the two catalytic solutions of complexes **C1** and **C2** after 2 hours of bulk electrolysis. The results show no correlation.

S12. References:

1. N. F. Chilton, R. P. Anderson, L. D. Turner, A. Soncini and K. S. Murray, *J Comput Chem*, 2013, **34**, 1164–1175.
2. P. Murali Krishna, K. Hussain Reddy, J. P. Pandey and D. Siddavattam, *Transition Metal Chemistry*, 2008, **33**, 661–668.
3. Duward. Shriver and Peter. Atkins, *Inorganic Chemistry*, W.H. Freeman & Company, 2006.
4. P. Zanello and A. Cinquantini, *Transition Met. Chem.*, 1985, **10**, 370–374.